

1 **Septin-microtubule association requires a MAP-like motif unique to Sept9 isoform 1**  
2 **embedded into septin octamers**

3

4

5 Mira Kuzmić<sup>1</sup>, Gerard Castro Linares<sup>2</sup>, Jindřiška Leischner Fialová<sup>1, 3\*</sup>, François Iv<sup>4</sup>, Danièle  
6 Salaün<sup>1</sup>, Alex Llewellyn<sup>4</sup>, Maxime Gomes<sup>4</sup>, Mayssa Belhabib<sup>4</sup>, Yuxiang Liu<sup>5</sup>, Keisuke Asano<sup>5</sup>,  
7 Taro Tachibana<sup>5,6</sup>, Gijsje Koenderink<sup>2\*\*</sup>, Ali Badache<sup>1\*\*</sup>, Manos Mavrakis<sup>4\*\*</sup>, Pascal Verdier-  
8 Pinard<sup>1\*\*</sup>

9

10 <sup>1</sup>Centre de Recherche en Cancérologie de Marseille (CRCM), INSERM, Institut Paoli-Calmettes, Aix  
11 Marseille Univ, CNRS, 13009 Marseille, France

12

13 <sup>2</sup>Department of Bionanoscience, Kavli Institute of Nanoscience Delft, Delft University of Technology,  
14 2629 HZ Delft, The Netherlands

15

16 <sup>3</sup>Department of Pathological Physiology, Faculty of Medicine, Masaryk University, Brno, Czech  
17 Republic

18

19 <sup>4</sup>Institut Fresnel, CNRS UMR7249, Aix Marseille Univ, Centrale Marseille, 13013 Marseille, France

20

21 <sup>5</sup>Department of Bioengineering, Graduate School of Engineering, Osaka City University, Osaka,  
22 Japan

23

24 <sup>6</sup>Cell Engineering Corporation, Osaka, Japan

25

26 \*current affiliation: Department of Biology, University of Copenhagen, Copenhagen, Denmark

27

28 \*\*Corresponding authors

29

30

31

32

33

34

35

36

37

38

39

40

41

42

43

44

45

46

47  
48  
49  
50  
51  
52  
53  
54  
55  
56  
57  
58  
59  
60  
61  
62  
63  
64  
65  
66  
67  
68  
69  
70  
71  
72  
73  
74  
75  
76  
77  
78  
79  
80  
81  
82  
83  
84  
85  
86  
87  
88  
89  
90  
91  
92

## Abstract

Septins, a family of GTP-binding proteins assembling into higher order structures, interface with the membrane, actin filaments and microtubules, which positions them as important regulators of cytoarchitecture. Septin 9 (Sept9), which is frequently overexpressed in tumors and mutated in hereditary neuralgic amyotrophy (HNA), mediates the binding of septins to microtubules, but the molecular determinants of this interaction remained uncertain. We demonstrate that a short MAP-like motif unique to Sept9 isoform 1 (Sept9\_i1) drives septin octamer-microtubule interaction in cells and *in vitro* reconstitutions. Septin-microtubule association requires polymerizable septin octamers harboring Sept9\_i1. Although outside of the MAP-like motif, HNA mutations abrogates this association, identifying a putative regulatory domain. Removal of this domain from Sept9\_i1 sequesters septins on microtubules, promotes microtubule stability and alters actomyosin fiber distribution and tension. Thus, we identify key molecular determinants and potential regulatory roles of septin-microtubule interaction, paving the way to deciphering the mechanisms underlying septin associated pathologies.

## 93 Introduction

94

95 Microtubules and actin filaments are cytoskeletal polymers involved in key cellular  
96 functions. Microtubules assemble from tubulin dimers to form hollow tubes that have the ability  
97 to switch between growing and shortening phases, a process called dynamic instability.  
98 Microtubule diversity arises, from tubulin isotypes, from post-translational modifications,  
99 including acetylation and glutamylation, often associated with stable sub-populations of  
100 microtubules, and from associations with specific microtubule-associated proteins (MAPs) that  
101 modulate microtubule dynamics<sup>1</sup>. Microtubules are critically involved in the segregation of  
102 chromosomes during cell division and the directed transport of various intracellular cargoes<sup>2</sup>.  
103 Actin monomers assemble into double helical strands that in cells are often cross-linked into  
104 bundles and networks<sup>3</sup>. In particular, the presence of associated myosins confers contractility to  
105 these actin fiber assemblies, that is essential during both cell division and migration. Such  
106 bundled actomyosin fibers form stress fibers that are qualified as peripheral and ventral when  
107 running near the cortex and the cell base, respectively. Stress fibers connect focal adhesions and  
108 the perinuclear actin cap linked to the top of the nucleus controlling its position and shape<sup>4</sup>.  
109 Several biological processes depend on the coordinated regulation of the actin and microtubule  
110 cytoskeletons, mediated by a diversity of molecular crosstalk between the two cytoskeletons.  
111 Direct and indirect contacts are involved, for instances, in cytokinetic furrow positioning, cell  
112 migration steering or maturation of neuronal dendritic spines<sup>5</sup>.

113 Septins are GTP-binding protein that form heteropolymeric complexes associating with  
114 membranes, actin filaments and a subset of microtubules<sup>6</sup>. Like yeast and *Drosophila* septins,  
115 human septin hexameric and octameric protomers can polymerize into filaments<sup>7-13</sup>. Septins are  
116 thought to function as diffusion barriers for protein compartmentalization or as scaffolds for  
117 protein-protein interactions during cells division and in an increasing number of processes during  
118 interphase<sup>14-16</sup>. During cytokinesis, septins are recruited to the sub-membrane cortex by  
119 anillin<sup>17,18</sup> and co-localize with the constricting actomyosin ring, prior to the specification and  
120 the maintenance of the ingression furrow position by microtubules<sup>19,20</sup>. Septins appear also to  
121 control abscission<sup>17,21-25</sup> that achieves cell division. It is still unclear how human septins interface  
122 with microtubules and the acto-myosin networks. Septins form a collar structure at the neck of  
123 dendritic spines, nanotubule-like protrusions and micro-tentacles to guide microtubules<sup>26-29</sup>. In  
124 adherent cells, septins concentrate on ventral stress fibers, and occasionally on perinuclear  
125 microtubules, depending on the cell type. Despite studies showing that septins regulate the traffic  
126 of motor proteins, like kinesin, the binding of MAPs and the guiding of microtubules in  
127 polarizing epithelia<sup>30</sup>, the functional consequences of septin-microtubule interaction are still  
128 largely unknown.

129 The 13 human septin genes encode four protein sequence homology-groups named after  
130 Sept2, Sept6, Sept7 and Sept3; septins from each group interact with each other in a specific  
131 order to form hexamers and octamers<sup>22,31,32</sup>. Septin octamers differ from hexamers by the  
132 addition of septins from the Sept3 group, with their arrangement recently determined as Sept2-  
133 Sept6-Sept7-Sept3-Sept3-Sept7-Sept6-Sept2<sup>10,33</sup>. Septins include a conserved GTP-binding  
134 domain (G domain) flanked by variable N- and C-termini. Septins assemble by the G domain on  
135 one side forming the G:G interface and by the N- and C- termini forming the NC:NC interface  
136 on the opposite side. This results in (NCSept2<sub>G:G</sub>Sept6<sub>NC:NC</sub>Sept7<sub>G:G</sub>Sept7<sub>NC:NC</sub>Sept6<sub>G:G</sub>Sept2<sub>NC</sub>)  
137 hexamers and (NCSept2<sub>G:G</sub>Sept6<sub>NC:NC</sub>Sept7<sub>G:G</sub>Sept3<sub>NC:NC</sub>Sept3<sub>G:G</sub>Sept7<sub>NC:NC</sub>Sept6<sub>G:G</sub>Sept2<sub>NC</sub>)  
138 octamers that can polymerize via a universal Sept2<sub>NC:NC</sub>Sept2 interface, that is labile in presence

139 of high salt concentrations. In the Sept3 group, Sept9 has been the most studied because it is  
140 ubiquitously expressed, and often overexpressed in tumors<sup>34</sup>. Interestingly Sept9 is mutated in a  
141 large number of hereditary neuralgic amyotrophy (HNA) patients<sup>35-37</sup>. Alternative splicing  
142 resulting in alternative translation start sites gives rise to five Sept9 isoforms (Sept9\_i1 to\_i5)  
143 differing by the length and/or sequence of their N-terminus and by their functions<sup>38-40</sup>. Sept9\_i1,  
144 \_i2 and \_i3 long isoforms share a common structurally disordered N-terminal domain (common  
145 N-ter) that was proposed, based on *in vitro* studies, to mediate binding to microtubules<sup>41</sup>.  
146 However, several studies indicate that only the isoform 1 of Sept9 (Sept9\_i1) drives the  
147 association of septins with microtubules<sup>24,32,40,42</sup>. In order to understand the contribution of  
148 septin-microtubule interaction to cell physiology and disease, it is critical to identify and  
149 characterize precisely the molecular determinants of this interaction.

150  
151 In the present study, we show that septin association with microtubules requires a MAP-  
152 like motif specific of Sept9\_i1 and the integration of Sept9\_i1 within polymerized septin  
153 octamers. *In vitro* reconstitution allowed us to demonstrate a direct and specific interaction of  
154 Sept9\_i1-harboring septin octamers with microtubules, which slows down depolymerization of  
155 microtubules. Based on this molecular characterization, we designed specific genetic variants,  
156 including HNA-like mutations, which modulate Sept9\_i1-microtubule interaction and we show  
157 that relocalizing septins to microtubules disturbs stress fiber distribution and tension.

## 158 159 **Results**

160  
161 **Different Sept9 isoform expression profiles are associated with distinct**  
162 **octamers/hexamers ratios and cytoskeletal localization.** We have analyzed septin expression  
163 profiles in commonly used cell models, namely U2OS osteosarcoma, HeLa cervical carcinoma  
164 cells, RPE1 retinal epithelial cells and SKBr3 breast carcinoma cells (Fig. 1a). Sept7 being  
165 unique in its group, it is essential for the formation of hexamers and octamers (Supplementary  
166 Fig. 1d). The four cell lines examined expressed very similar levels of Sept7. In the Sept2 group,  
167 Sept2 was expressed in all cell lines and Sept5 was only detected in U2OS cells. Expression of  
168 septins from the Sept6 group was more variable, except for Sept8 that was expressed at similar  
169 levels in all cell lines. U2OS and HeLa cells expressed similar levels of total Sept9. However,  
170 U2OS cells expressed mostly isoform 3, whereas HeLa cells expressed mostly isoform 1. RPE1  
171 and SKBr3 cells expressed higher levels of Sept9 with similar levels of Sept9\_i1 and Sept9\_i2,  
172 and no or very low levels of Sept9\_i3.

173 To assess how Sept9 expression profiles affected its incorporation in septin hexamers and  
174 octamers, we extracted cells in conditions that preserved oligomers and performed native gel  
175 electrophoresis and analysis by Western blotting (Fig. 1b and Supplementary Fig. 1). Based on  
176 the detection of the essential Sept7 and pan-expressed Sept8, U2OS and HeLa cells contained  
177 more hexamers than octamers, as opposed to RPE1 and SKBr3 cells. This result is consistent  
178 with higher Sept9 expression levels in RPE1 and SKBr3 leading to higher levels of octamers. In  
179 addition, our results indicate that long Sept9 isoforms incorporate indifferently in octamers. We  
180 did not detect smaller septin assemblies containing Sept9 monomers or dimers, suggesting that,  
181 at endogenous levels, the entire pool of Sept9 is stably incorporated into octamers.

182 Next, we examined the localization of Sept9 in these cell lines either in interphase or in  
183 late cytokinesis (Fig. 1c, d). We observed that Sept9 was associated with actin fibers in all  
184 interphase cells, especially on ventral stress fibers (Fig. 1c, d). Interestingly, consistent with

185 previous observation<sup>40</sup>, Sept9 co-localized with a subpopulation of acetylated microtubules in  
186 HeLa and SKBr3 cells; in cytokinetic cells, Sept9 concentrated cortically at the ingression  
187 furrow and on the thick bundles of acetylated microtubules contained in the intercellular bridge.  
188 In U2OS cells, which express primarily Sept9\_i3, septins associated with the actin cytoskeleton  
189 but did not co-localize with microtubules. These results indicate that the association of septins  
190 with microtubules is dependent on the presence of octamers harboring Sept9\_i1. It is less clear  
191 why in RPE1 cells, despite Sept9\_i1 levels comparable to SKBr3 cells, there was no association  
192 of Sept9 with microtubules, except in primary cilia (Fig. 1e).

193  
194 **Sept9\_i1 interacts with microtubules via a specific MAP-like motif.** The fact that  
195 only Sept9\_i1, but not the closely related i2 and i3 isoforms, is required for septins to bind  
196 microtubules identifies the sequence formed by the first specific 25 amino acid residues of the  
197 Sept9\_i1 protein, as specific to this isoform and as key for its interaction with microtubules<sup>40</sup>.  
198 This sequence being well conserved in vertebrates (Supplementary Fig. 2), it is also indicative of  
199 an important function. Searching for similar sequences in proteins related to the microtubule  
200 cytoskeleton by using the NCBI Blastp tool, we found the Arabidopsis thaliana AIR9 protein, a  
201 plant MAP involved in cytokinesis<sup>43</sup>. The sequence of AIR9 similar to the Sept9\_i1 specific  
202 sequence was located in the AIR9-microtubule binding domain (AIR9 1-234)<sup>43</sup>. Alignment of  
203 these two sequences reveals a block of similar sequence that we named AIR-9-like (Fig. 2a).  
204 Another sequence, located upstream in the AIR9 N-terminus (aa 46-78), presents a lower  
205 similarity with the Sept9\_i1 specific sequence (Fig. 2a). Strikingly, the AIR9-like block had  
206 similarities with canonical repeats found in the microtubule binding domains (MBDs) of the  
207 structural human MAPs, tau, MAP2 and MAP4, which are known to interact directly with the  
208 surface of microtubules (Fig. 2a). An upstream smaller block in the Sept9\_i1 specific sequence  
209 showed similarities with the MAP4 R2 repeat. Thus, Sept9\_i1 displays a putative MBD, similar  
210 to the MBD repeats of several MAPs and constituted by a MAP4 R2-like sequence followed by  
211 an AIR9-like sequence.

212 To unequivocally demonstrate that this motif is actually the MBD of Sept9\_i1, we  
213 examined the localization of Sept9\_i1 mutants (C-terminally tagged with GFP), presenting  
214 deletions or point mutations in the first 25 amino acid residues (Fig. 2b), in U2OS cells (Fig. 2c,  
215 d and Supplementary Fig. 3a-c). U2OS cells were chosen because they express very low levels  
216 of Sept9\_i1 (Fig. 1a), and show no Sept9-microtubule co-localization (Fig. 1c, d). In addition,  
217 U2OS cells were amenable to simultaneous siRNA-mediated knockdown (KD) of Sept9 and  
218 expression of exogenous Sept9\_i1-GFP constructs at near-endogenous Sept9 levels  
219 (Supplementary Fig. 3a). Wild type Sept9\_i1 co-localized with actin in all cells and with  
220 microtubules in more than 60% of the cells. Sept9\_i3 and the  $\Delta$ 1-25 Sept9\_i1 mutant also  
221 associated with actin fibers, but never localized to microtubules (Fig. 2c, d, f and Supplementary  
222 Fig. 3b, d). This result is consistent with our previous observations of Sept9\_i3 and Sept9\_i1  $\Delta$ 1-  
223 25 vs Sept9\_i1 localization in SKBr3 cells (using N-terminally tagged constructs)<sup>40</sup>. Deletion of  
224 the AIR9-like portion ( $\Delta$ 10-25 mutant) or of the MAP4 R2-like portion ( $\Delta$ 1-7 mutant) totally or  
225 largely abrogated Sept9 binding to microtubules, respectively (Fig. 2c and Supplementary Fig.  
226 3b). Next, we introduced point mutations in the AIR9-like portion (Fig. 2b). Independent  
227 mutations of two sets of contiguous serine residues (S12A/S13A and S22A/S23A), conserved in  
228 the AIR9 MBD, did not significantly alter the co-localization of Sept9 with microtubules (Fig.  
229 2c, d and Supplementary Fig. 3b, c). Importantly, mutations of the two arginine residues  
230 (R10A/R15A), conserved in all vertebrates (Supplementary Fig. 2) and present in the AIR9

231 MBD, completely abrogated the binding of Sept9 to microtubules (Fig. 2c, d and Supplementary  
232 Fig. 3b, c). Collectively, our data show that the Sept9\_i1 specific N-terminal sequence is an  
233 MBD analogous to the ones found in human MAPs and the plant AIR9 MAP. Of note, in  
234 contrast to MAP MBDs, the Sept9\_i1 specific sequence is not tandem-repeated and lacks  
235 upstream conserved residues (Fig. 2a).

236 A previous report proposed, based on *in vitro* studies using recombinant polypeptides,  
237 that Sept9\_i1<sub>61-113</sub> within the N-terminal region common to all Sept9 long isoforms (i1, i2 and i3)  
238 was the main contributor to microtubule binding<sup>41</sup>. To evaluate a potential contribution of Sept9  
239 N-terminal region common to all long isoforms (common N-ter), we generated a chimeric Sept9  
240 deleted of the entire common N-ter by fusing the isoform 1 specific sequence to Sept9\_i5, the  
241 shortest Sept9 isoform, and named it Sept9\_i1-i5 (Fig. 2e). Whereas Sept9\_i5 localized strictly to  
242 actin fibers (Fig. 2f, h and Supplementary Fig. 3e), its fusion to the Sept9\_i1 specific motif was  
243 sufficient to localize septins to microtubules in all interphase cells. Surprisingly, this was  
244 accompanied by the complete loss of Sept9 co-localization with actin fibers (Fig. 2f, h).  
245 Consistent with these findings, expression of Sept9\_i1-i5 during cytokinesis increased strongly  
246 the percentage of cells showing Sept9 association with microtubule bundles at the intercellular  
247 bridge (Supplementary Fig. 3d).

248 Our results demonstrate that the Sept9\_i1 MBD is required and sufficient to target Sept9  
249 to microtubules, whereas the N-terminal region common to all long isoforms is dispensable.  
250 Interestingly the Sept9\_i1-i5 is much more efficient than Sept9\_1 for targeting septins to  
251 microtubules (Fig. 2f, h and Supplementary Fig. 3d), hinting that the common N-ter might have a  
252 negative regulatory function. Sept9 is mutated in hereditary neuralgic amyotrophy (HNA)  
253 patients. HNA-associated mutations are located in the Sept9 common N-ter<sup>35</sup>, but their impact on  
254 Sept9 function remains to be elucidated. We introduced separately the two most frequently  
255 described HNA mutations (R106W or S111F) in Sept9\_i1 constructs and evaluated their impact  
256 on Sept9\_i1 localization. Both Sept9\_i1 R106W and S111F maintained co-localization with  
257 ventral stress fibers (Fig. 2g, h). However, both mutations suppressed the association with  
258 microtubules (Fig. 2g, h). This result confirms that the common N-ter, while not required for  
259 Sept9 microtubule binding per se, is an important regulatory domain and provides novel insights  
260 into the molecular etiology of HNA.

261  
262 **Sept9\_i1 must be included in a polymerized septin octamer to associate with**  
263 **microtubules.** In contrast to typical MBDs in structural MAPs, the Sept9\_i1 specific sequence  
264 does not have tandem repetitions. We hypothesized that the dimerization of Sept9\_i1 in octamers  
265 via the NC interface brings two Sept9\_i1 specific sequences in close proximity, to form a MBD  
266 mimicking tandem arrangements of repeats. To test this hypothesis and the oligomeric  
267 environment required for microtubule binding, we introduced point mutations into Sept9\_i1 that  
268 should disturb the NC interface to generate tetramers, or the G interface to generate non-  
269 incorporated Sept9\_i1<sup>31</sup> (Fig. 3a). We then expressed these constructs in U2OS cells in place of  
270 endogenous Sept9 (KD via siRNA). Importantly, re-expression of wild type Sept9\_i1-GFP  
271 restored close to endogenous levels of octamers and hexamers (Fig. 3a). As expected, most of the  
272 Sept9\_i1 G interface mutant (Sept9\_i1 G<sub>mut</sub>) did not incorporate in octamers (Fig. 3a). Instead, it  
273 migrated with an apparent molecular weight of 138 kDa, corresponding most likely to  
274 monomeric Sept9\_i1, whose gel motility is retarded by the long and disordered N-terminus<sup>32</sup>  
275 (Supplementary Fig. 1a). Based on previous studies<sup>22,31,44</sup>, we generated two Sept9\_i1 NC  
276 interface mutants with mutations in the  $\alpha 0$  helix either in the basic residue stretch (Sept9\_i1

277 NC<sub>mut1</sub>) or upstream of this stretch in key hydrophobic residues (Sept9\_i1 NC<sub>mut2</sub>). Sept9\_i1  
278 NC<sub>mut1</sub> incorporated in tetramers and Sept9\_i1 NC<sub>mut2</sub> incorporated partly in tetramers, but  
279 mostly migrated like the monomeric protein (Fig. 3a), indicating that mutations in Sept9\_i1  
280 NC<sub>mut2</sub> might affect both NC and G interfaces. Importantly, we observed no association of  
281 Sept9\_i1 G or NC mutants with microtubules, but rather a diffuse cytosolic distribution (Fig. 3b).  
282 These results show that neither septin tetramers nor Sept9\_i1 monomers bind to microtubules,  
283 and that the octameric septin context, which brings together two Sept9 units via their NC  
284 interface, is mandatory for Sept9\_i1 association with microtubules.

285 Next, we evaluated if septin octamers harboring Sept9\_i1 bind microtubules by  
286 themselves or if they need to assemble into longer polymers via Sept2:Sept2 NC interfaces.  
287 Mutation of the Sept2 NC interface<sup>31,45</sup> (Sept2 NC<sub>mut</sub>) should produce a mixture of isolated  
288 octamers and hexamers in cells (Fig. 3c). To evaluate its impact on Sept9\_i1 localization, we  
289 knocked down both Sept9 and Sept2, and re-expressed Sept9\_i1 (tagged with GFP to monitor  
290 Sept9 localization), together with wild type or Sept2 NC<sub>mut</sub> (tagged with mApple to identify  
291 transfected cells). Using native gel separation, we verified that wild type Sept2 and Sept2 NC<sub>mut</sub>  
292 generated the same relative expression levels of octamers and hexamers (Fig. 3c). However,  
293 when Sept2 NC<sub>mut</sub> was expressed Sept9\_i1 (and Sept2) no longer co-localized with microtubules  
294 (Fig. 3d). Thus, the association of Sept9\_i1 with microtubules requires its incorporation in  
295 polymerizable octamers.

296  
297 **Sept9\_i1 associates with stable microtubules.** Because of the sequence similarities  
298 between Sept9\_i1 and MAP4 MBDs, the two proteins might use the same tubulin interdimer  
299 binding pocket at the surface of microtubules<sup>46,47</sup>. At endogenous Sept9\_i1 levels in SKBr3 cells,  
300 we observed that MAP4 associated with the entire microtubule cytoskeleton, whereas Sept7 was  
301 concentrated on acetylated bundled microtubules (Fig. 4a). In U2OS cells transfected with  
302 Sept9\_i1, the same differential distribution between MAP4 and Sept9\_i1 was observed. When  
303 the Sept9\_i1-i5 chimera, which showed a stronger affinity for microtubules, was expressed,  
304 MAP4 was absent on many microtubule bundles (Fig. 4b). These observations suggest that the  
305 binding sites of Sept9\_i1 MBD and MAP repeats partially overlap on the microtubule lattice.

306 As we repeatedly observed the preference of Sept9\_i1 for acetylated microtubules (Fig.  
307 1d, e, Fig. 2d, h, Fig. 3b, d, Fig. 4a and Supplementary Fig. 3c, g), we wondered whether  
308 microtubule acetylation was a determinant of septin binding. We first examined whether the  
309 unexpected lack of Sept9\_i1 association with microtubules in RPE1 cells (Fig. 1c, d) was  
310 associated with a deficit of microtubule acetylation. Tubulin acetylation levels in RPE1 cell line  
311 were indeed low, especially compared to those in another retina epithelial cell line (ARPE19),  
312 which expressed similar levels of Sept9\_i1 (Fig. 5a) but showed frequent septin association with  
313 microtubules (Fig. 5b, supplementary Fig. 3f). Other posttranslational modifications (PTMs) of  
314 tubulins, such as polyglutamylation, that could affect Sept9\_i1 binding<sup>48,49</sup> were equally low in  
315 these cell lines (Fig. 5a). Moreover, treating RPE1 cells with paclitaxel, a drug that induces  
316 acetylation and bundling of microtubules in cells, induced the association of septins with  
317 microtubules (Fig. 5c). Of note, the paclitaxel-driven re-localization of septins to microtubules  
318 was dependent on the expression of Sept9\_i1 (Fig. 4c and Fig. 5c). Thus, Sept9\_i1 association  
319 with microtubules appears to be correlated with tubulin acetylation. To determine if paclitaxel-  
320 induced tubulin acetylation was responsible for re-localization of septins on microtubules,  
321  $\alpha$ TAT1, the major tubulin acetyl transferase<sup>50</sup>, was knocked down to prevent tubulin acetylation,  
322 prior to paclitaxel treatment (Fig. 5d). This experiment clearly showed that re-localization of

323 septins on paclitaxel-bundled microtubules was independent of tubulin acetylation levels (Fig.  
324 5d).

325 Finally, we evaluated whether Sept9\_i1, like MAPs, contributes to microtubule  
326 stabilization in the presence of nocodazole, a microtubule-depolymerizing agent. We observed  
327 that, whereas Sept9\_i1 moderately stabilized microtubules, Sept9\_i1-i5 strongly promoted the  
328 resistance of microtubules against nocodazole-induced depolymerization (Fig. 4c, d and  
329 Supplementary Fig. 3g). Of note, depolymerization of microtubules allowed Sept9\_i1-i5 to re-  
330 localize to actin fibers in nearly 60% of the cells (Fig. 4c).

331 Collectively, these data establish that septin octamers harboring Sept9\_i1 associate with a  
332 population of stable bundled microtubules in cells, independently of their acetylation levels, and  
333 contribute to microtubule stabilization.

334  
335 **Recombinant septin octamers harboring Sept9\_i1 interact directly and specifically**  
336 **with microtubules and slow down their depolymerization.** In order to assess if recombinant  
337 octamers harboring (Oct\_9i1) are able to bind directly to microtubules, we purified recombinant  
338 septin octamers (Sept2-Sept6-Sept7-Sept9\_i1-Sept9\_i1-Sept7-Sept6-Sept2 and Sept2-Sept6-  
339 Sept7-Sept9\_i3-Sept9\_i3-Sept7-Sept6-Sept2)<sup>12</sup> (Supplementary Fig. 1b) and reconstituted  
340 dynamic microtubules made from purified tubulin  $\alpha/\beta$ -heterodimers in the presence of each type  
341 of octamer. Total internal reflection fluorescence (TIRF) microscopy allowed visualizing both  
342 dynamic microtubules incorporating rhodamine-tagged tubulin and septin oligomers  
343 incorporating GFP-tagged Sept2 (Fig. 6a). Microtubules were polymerized from a 10  $\mu$ M tubulin  
344 heterodimer solution and in the presence of 10 to 300 nM of octamers, i.e. at concentrations  
345 comparable to the tubulin  $\alpha/\beta$ -heterodimer ( $\sim$ 10  $\mu$ M) and septin complex ( $\sim$ 400 nM)  
346 concentrations measured in HeLa cells<sup>51</sup>.

347 We clearly observed Oct\_9i1 binding to microtubules at the lowest concentration (10 nM,  
348 Fig. 6b, c). Oct\_9i1 diffused randomly on the lattice of dynamic microtubules (Fig. 6c and  
349 Supplementary Movie 1), and were also on the stable microtubule seeds. On kymographs,  
350 diffusion on microtubules during the growing phases was clearly apparent, with a reduced  
351 presence on the microtubule seeds (Fig. 6c). Of note, upon microtubule depolymerization,  
352 Oct\_9i1 accumulated and remained on seeds, then diffused again on the microtubule upon its  
353 regrowth (Fig. 6c). At 10 nM concentration, there were no detectable recombinant octamers  
354 harboring Sept9\_i3 (Oct\_9i3) on dynamic or stable seed microtubules. Decoration of  
355 microtubules increased with increasing concentrations of Oct\_9i1, until saturation at 300 nM  
356 (Fig. 6b, c and Supplementary Movie 1). In comparison, Oct\_9i3 only showed significant  
357 binding at the highest concentration (300 nM), which was restricted to the stable microtubule  
358 seeds (Fig. 6b, c and Supplementary Movie 2). Altogether these results indicate that octamers  
359 harboring Sept9\_i1 bind specifically and directly dynamic individual microtubules.

360 We then analyzed how the addition of Oct\_9i1 or Oct\_9i3, at 10 to 300 nM, affected  
361 parameters of microtubule dynamic instability (Fig. 7a, b). Both types of octamer were similarly  
362 and moderately affecting microtubule growth rate at intermediate concentrations. Strikingly,  
363 Oct\_9i1 induced a strong and dose-dependent decrease of the microtubule shortening rate, while  
364 Oct\_9i3 had no effect, even when used at the highest concentration. The catastrophe time  
365 frequency was not consistently altered by the addition of either types of octamer. Intriguingly,  
366 we observed that, solely in the presence of 200 nM or 300 nM of Oct\_9i1, about 10% of  
367 depolymerizing microtubules had an unusual curved tubulin-containing structure at their plus-  
368 end that was decorated by septins (Fig. 7c and Supplementary Movie 3). These structures could

369 be made of few protofilaments whose shortening is slowed down by the association with  
370 Oct<sub>9i1</sub>.

371

372 **Re-localization of octamers from stress fibers to microtubules alters stress fiber**  
373 **organization and function.**

374 Our observations indicate that the population Sept9<sub>i1</sub> octamers associate with both  
375 microtubules and actin fibers and can shuttle between them. This was for instance illustrated by  
376 the observation that the Sept9<sub>i1-i5</sub> chimera co-localized with microtubules only (Fig. 2f, h and  
377 Fig. 4b, c), but was able to co-localize with actin fibers upon nocodazole-induced  
378 depolymerization of microtubules (Fig. 4c). Thus, beyond its direct contribution to microtubule  
379 stability and dynamics (this study) and microtubule-linked processes, e.g. cell resistance to  
380 paclitaxel<sup>52</sup>, the relative distribution of Sept9<sub>i1</sub> on microtubules vs actin fibers might indirectly  
381 affect actomyosin fibers distribution and cellular events dependent on their contractility.  
382 Previous studies showed that Sept9 associates with perinuclear actin fibers, especially ventral  
383 stress fibers whose organization depends on Sept9<sup>40,53</sup> (Supplementary Fig. 5a). We similarly  
384 observed that in U2OS (Fig. 8a) and RPE1 cells (Supplementary Fig 5d), the knockdown of  
385 Sept9 strongly decreased the percentage of cells with sub-nuclear stress fibers. To test the  
386 hypothesis that septin octamer association with microtubules impacts actin fiber organization and  
387 function, we generated U2OS cell lines stably expressing Sept9<sub>i1</sub> variants (Supplementary Fig.  
388 4).

389 Expression of Sept9<sub>i1-i5</sub>, only associating with microtubules, was concomitant with the  
390 strong reduction in the percentage of cells having sub-nuclear stress fibers (Fig. 8b), while  
391 expression of Sept9 constructs with no or reduced microtubule association (Sept9<sub>i1</sub>  $\Delta$ 1-25,  
392 Sept9<sub>i1</sub> R10A/R15A and Sept9<sub>i3</sub>) preserved sub-nuclear stress fibers (Fig.8b). Likewise,  
393 paclitaxel-induced re-localization of Sept9<sub>i1</sub> octamers from stress fibers to microtubule bundles  
394 in RPE1 cells induced the loss of sub-nuclear stress fibers (Fig. 5c), whereas paclitaxel-treatment  
395 of U2OS expressing Sept9<sub>i3</sub> as the major isoform did not result in any loss of sub-nuclear stress  
396 fibers (Fig. 5c). Thus, the sequestration of septin octamers on microtubules is dependent on the  
397 MBD of Sept9<sub>i1</sub> and induces a loss of sub-nuclear stress fibers. These results suggest that the  
398 precise relative distribution of septins on microtubules vs on actin fibers is critical for an intact  
399 actin cytoskeleton.

400 As a functional assay for testing the interplay between Sept9<sub>i1</sub>-microtubule association  
401 and stress fiber function, we plated U2OS cells KD for Sept9 or expressing different Sept9<sub>i1</sub>  
402 variants on adhesive micropatterns. Indeed, when plated on adhesive micropatterns, cells form  
403 actin stress fibers across adhesives edges, and the convexity of the non-adhesive cell edges  
404 provides a readout for stress fiber tension<sup>54</sup>. Partial or total localization of septins on  
405 microtubules vs stress fibers in U2OS cells stably expressing Sept9<sub>i1</sub> or Sept9<sub>i1-i5</sub>,  
406 respectively, promoted the concavity of non-adhesive cell edges, reflective of the relaxation of  
407 peripheral stress fibers compared to cells stably expressing Sept9<sub>i1</sub>  $\Delta$ 1-25, that is solely located  
408 on actin fibers (Fig. 8c). The knockdown of Sept9 in U2OS cells, leading to the loss of septin  
409 octamers, induced a similar detectable relaxation of peripheral stress fiber (Fig. 8d).

410

411 Altogether, these results suggest that the relative abundance of octamers vs hexamers  
412 and/or the relative proportion of septin octamers able to associate to microtubules contribute  
413 critically to the maintenance of the actomyosin organization and tension. Our study indicates that  
414 the propensity of octamers harboring Sept9<sub>i1</sub> to associate with microtubule depends on

415 Sept9\_i1 expression levels, the state of its N-terminal regulatory domain, and the extent of  
416 microtubule bundling.

417

## 418 **Discussion**

419

420 Septins associate in a dynamic way with different major constituents of the cell, i.e.  
421 membranes, actin fibers and microtubules<sup>6</sup>. Septin octamers and hexamers co-associate to form  
422 septin filaments<sup>7,8,10-13</sup>, whose properties may depend in part on the relative abundance of  
423 incorporated octamers and hexamers. In addition, the expression profile of different septin  
424 isoforms, including those of Sept9, may direct both localization and function of septin octamers.  
425 It is thus critical to define precisely the molecular basis of the different subcellular localizations  
426 of septin complexes, in order to develop tools differentially altering their distribution. This will  
427 help us understand how the different septin pools respectively contribute to cell physiology and  
428 pathology.

429 Earlier studies have shown that Sept9\_1 has a preferential affinity for microtubules in  
430 cells<sup>24,32,40,42</sup> indicating that the first 25 aa residues defining the sequence unique to this long  
431 isoform was responsible for specific binding to microtubules. In the present study, we identify a  
432 conserved MAP-like MBD in Sept9\_i1, including two distinct modules and key conserved  
433 residues whose mutation abrogates microtubule binding. We and others have identified imperfect  
434 repeats containing basic amino acid residues in the common long N-terminal sequence of  
435 Sept9\_i1, \_i2 and \_i3<sup>40,41</sup>. These repeats were proposed to constitute the MBD of Sept9 via  
436 electrostatic interactions with the acidic C-termini of  $\beta$ -tubulin exposed at the surface of  
437 microtubules<sup>41</sup>, in line with the accepted mode of interaction of conventional MAPs at the time<sup>55</sup>.  
438 However, recent advances in the determination of the structure of MAP tandem repeats bound to  
439 microtubules by cryo-EM contradicted this model<sup>46,47</sup>. These studies revealed that a sequence in  
440 Tau and MAP4 repeats anchors MAPs to a binding pocket at the interface between consecutive  
441 tubulin heterodimers in protofilaments, independently of tubulin acidic C-termini. We actually  
442 found numerous similarities between the MAPs repeated sequences and the AIR9-like module of  
443 Sept9\_i1 MBD, that are not present in the repeats shared with the other Sept9 long isoforms.  
444 Most importantly, our data show that, contrary to the Sept9\_i1 MBD, the N-terminal region  
445 common to all long isoforms is not required for the association of Sept9\_i1 harboring octamers  
446 with microtubules in cells. Deletion of this region actually favored septin association with  
447 microtubules at the expense of actin fibers. These findings led us to speculate that the common  
448 N-terminal domain is not directly involved in the interaction of Sept9\_i1 with the microtubule  
449 lattice, but negatively regulates it. The imperfect repeats of the common N-terminal domain were  
450 predicted to form short  $\beta$ -sheets whereas the rest of the domain is disordered<sup>40</sup>. One of the  
451 imperfect repeats of the common N-terminal region is the locus of mutations detected in HNA  
452 patients<sup>35-37</sup>. To this date the mechanisms whereby Sept9 mutations contribute to this disease are  
453 not known. Remarkably, when we expressed Sept9\_i1 harboring HNA-like mutations, septin  
454 octamers were no longer able to associate with microtubules, while still associating with actin  
455 fibers. This finding suggests that HNA-associated mutations alter the putative “Sept9\_i1 MBD  
456 regulatory region” providing clues for the determination of the molecular mechanisms  
457 underlying HNA.

458 Importantly, we demonstrated that Sept9\_i1 localizes septins on microtubules, only if it is  
459 included in polymerizable septin octamers. At endogenous expression levels, in the diverse  
460 cellular models we studied, we did not observe the presence of a significant pool of monomeric

461 Sept9 (Fig. 1b), which suggests that microtubule-associated Sept9 is wholly incorporated in  
462 octamers in these cells. Conversely, the large excess of Sept9\_i1 monomers in cells expressing  
463 the Sept9\_i1 G interface mutant was not associated with microtubules (Fig. 3a, b). Thus, *in vitro*  
464 studies with isolated recombinant Sept9\_i1 suggesting that Sept9\_i1 can binds and bundle  
465 microtubules by itself<sup>41,56,57</sup> must be interpreted with caution.

466 In previous studies, recombinant Sept9\_i3 or the common N-ter fragments were shown to  
467 associate with microtubules, assembled from purified tubulin<sup>41,56</sup>. The discrepancy is most likely  
468 linked to the fact that in these *in vitro* experiments, Sept9 was used outside of its natural  
469 octameric context, often at high concentrations (up to 10-30  $\mu$ M in pelleting assays) and using  
470 paclitaxel or GMPCPP stabilized microtubules in very low salt buffers, which likely favored  
471 electrostatic interactions. Using recombinant octamers harboring Sept9\_i1 and Sept9\_i3<sup>12</sup>, we  
472 observed that only those harboring Sept9\_i1 associated with dynamics microtubules at low  
473 nanomolar concentrations, *in vitro*. Our *in vitro* reconstitution experiments results are the first  
474 one to recapitulate the specific binding of Sept9\_i1 octamers to microtubules observed in cells  
475 here and by others<sup>40,52</sup>. Of note, although recombinant Sept2-Sept6-Sept7-Sept7-Sept6-Sept2  
476 hexamers were found to interact with microtubules *in vitro*<sup>58</sup>, this is not consistent with the  
477 absence of co-localization of septin hexamers with microtubules, when Sept9 was knocked down  
478 in cells<sup>40</sup> (Fig 8a and Supplementary Fig. 1d).

479 Septins associate with a sub-population of bundled microtubules<sup>41,42,59</sup>. We confirm that  
480 Sept9\_i1 co-localize with acetylated, bundled microtubules (much more selectively than  
481 structural MAPs, such as MAP4). As we also show that microtubule acetylation is not a  
482 requirement, Sept9\_i1 binding appears rather to rely on microtubule bundling in cells.  
483 Intriguingly, microtubule bundling is not required *in vitro*. This paradox will require other  
484 studies, including structural ones, to further characterize the molecular bases of the association of  
485 septins with individual and bundled microtubules.

486 Our data show that octamers harboring Sept9\_i1 slowed down microtubule  
487 depolymerization *in vitro* and stabilized microtubules in cells treated with nocodazole. It will be  
488 important to determine how these molecular events contribute to microtubule-dependent cellular  
489 processes such as spatiotemporal sorting of vesicles and organelles<sup>48,57</sup>, formation of protrusive  
490 structures<sup>26-29,60,61</sup> or cell survival against cytotoxic doses of paclitaxel<sup>52</sup>.

491 Association of septins with microtubules is likely to be regulated by cell- and tissue-  
492 specific contexts. Indeed, septin association with microtubules is clearly correlated to the specific  
493 expression of the Sept9\_i1 isoform and is sensitive to the bundling state of microtubules. Septin-  
494 microtubule interaction might also be modulated by the presence of competing MAPs or PTMs  
495 targeting the Sept9\_i1 MBD and/or its putative regulatory domain. Importantly, we show that  
496 deficient Sept9\_i1 binding to microtubules is associated with a diseased state, as two distinct  
497 HNA-like point mutations prevented Sept9 binding to microtubules. We are still far from  
498 understanding the underlying mechanism leading to HNA, which might be related to  
499 dysregulated microtubule function, but might be related also to an excessive association of  
500 septins with actin fibers and perturbation of actomyosin functions. Thus, our work not only  
501 establishes a new molecular basis for studying the physiological relevance of the association of  
502 septin with microtubules, but also open new avenues in the difficult search for the causative  
503 events leading to this rare neuropathy.

504  
505  
506

## 507 **Materials and methods**

508

### 509 **Human Cell lines.**

510 U2OS (ATCC), SKBR-3 (ATCC), HeLa (a kind gift from Dr Patrice Dubreuil, CRCM,  
511 Marseille, France), RPE-1 and ARPE19 (kind gifts from Dr Michael Sebbagh, CRCM,  
512 Marseille) cells were maintained in Dulbecco's modified Eagle's medium (DMEM) (Gibco)  
513 supplemented with 4 mM GlutaMAX™, 10 % fetal bovine serum (FBS) and 1% sodium  
514 pyruvate (supplemented DMEM), except ARPE19 cells that were cultivated in DMEM/F12 (1:1  
515 mixture of DMEM and Ham's F12, Gibco) supplemented as for DMEM. All cell lines were  
516 maintained in the presence of 5% CO<sub>2</sub> humidified atmosphere at 37°C. RPE-1 cells were also  
517 grown on coverslips coated with collagen (Corning, Cat#354236) until they reached confluency  
518 and ciliogenesis was induced by growing cells in DMEM containing only 0.5% of fetal bovine  
519 serum for 24 hours.

520

### 521 **Plasmids coding for fluorescent septin constructs and transfection**

522 To drive expression of the constructs in mammalian cells, we used the immediate early enhancer  
523 and promoter of human cytomegalovirus (CMV promoter, 508 base pairs). Human Sept9\_i1  
524 cDNA was a gift from C. Montagna (Albert Einstein College of Medicine, USA). Human  
525 Sept9\_i3 cDNA was a gift from W. Trimble (University of Toronto, Canada). A synthetic human  
526 Sept2 coding sequence (Eurofins Genomics, Germany) was generated using the codon usage of  
527 mouse Sept2 except for the five codons that differ between the two species, for which we used  
528 codons encoding the human residues. C-terminal green and red fluorescent protein fusions were  
529 generated using monomeric (V206K) superfolder GFP (msfGFP)<sup>62-65</sup> and monomeric Apple  
530 (mApple)<sup>64,66</sup>, respectively. All constructs were generated with two-insert seamless cloning (In-  
531 Fusion HD Cloning Plus Kit from Takara Bio, Cat# 638910) using NheI/BamHI linearized  
532 plasmid backbones (Addgene plasmid #54759) and the oligonucleotide primer sequences (listed  
533 in Supplementary Table 1). Primers for seamless cloning were Cloning Oligo (<60 bp) or  
534 EXTREmer (>60 bp) synthesis and purification quality from Eurofins Genomics, Germany.  
535 Restriction enzymes were FastDigest enzymes from Thermo Scientific. All plasmids were  
536 verified by sequencing (Eurofins Genomics, Germany) after each cloning step, including the  
537 midpreps used for plasmid production. Constructs were transiently transfected by nucleofection  
538 in U2OS cells (Amaxa nucleofector program U2OS X-001, Lonza) as described previously<sup>40</sup>.

539

### 540 **siRNAs and transfection**

541 The following 19-mer duplex siRNAs were purchased from LifeTechnologies: siRNA control  
542 (siCtrl) targeting the E.Coli  $\beta$  galactosidase (LacZ) (5'-GCGGCUGCCGAAUUUACC-3'),  
543 Sept9 (5'-GGAUCUGAUUGAGGAUAAA-3') targeting the 3'UTR of all human Sept9 mRNA  
544 variants, Sept7 (5'-CGACUACAUUGAUAGUAAA-3') targeting the human mRNA coding  
545 region,  $\alpha$ TAT1 (5'-CGCACCAACUGGCAAUUGA-3'), whose design was based on validated  
546 siRNA  $\alpha$ TAT1#2 from Shida et al<sup>67</sup>. Transfection of siRNA was performed as described  
547 previously<sup>40</sup> either with Lipofectamine RNAiMAX (Invitrogen, Cat# 13778075) or Amaxa cell  
548 line nucleofection kit V (Lonza, Cat#VCA-1003).

549

550

551

552

553 **Drug treatments**

554 For some experiments, cells were treated for two hours with 2  $\mu$ M paclitaxel (Sigma-Aldrich,  
555 Cat#T7191) or 10  $\mu$ M nocodazole (Sigma-Aldrich, Cat#M1404) in DMSO or with DMSO alone  
556 (Sigma-Aldrich, Cat#D8418).

557

558 **Antibodies**

559 Labeling of septins on Western blots (WB) and/or on immunocytochemistry coverslip (ICC) was  
560 achieved with the following antibodies: rabbit polyclonals against human Sept2 (Sigma-Aldrich,  
561 Cat#HPA018481, WB), against human Sept9 (Sigma-Aldrich, Cat#HPA042564 and  
562 HPA050627, WB and ICC; Proteintech, Cat#10769-1-AP, WB), against Septin 7 (IBL,  
563 cat#18991, WB and ICC), against Sept11 (Sigma-Aldrich, Cat#SAB2102111, WB), against  
564 human Sept5, against Sept8 (kind gifts from Barbara Zieger, University of Freiburg, Germany,  
565 WB), against Sept6 (a kind gift from Makoto Kinoshita (Nagoya University, Japan, WB), against  
566 Sept10 (Sigma, Cat#HPA047860, WB); rat monoclonals against human Sept9\_i1 (clone 4D2A5,  
567 WB) or human Sept9\_i3 (clone 1A6C2, WB), and against human Sept7 (clone 10A7, WB and  
568 ICC) were produced as described previously<sup>40</sup> (WB). Other antibodies were against  $\alpha$ -tubulin:  
569 mouse monoclonal (Sigma-Aldrich, DM1A Cat#05-829, WB and ICC), rat monoclonal  
570 (Invitrogen, YL1/2 Cat#MA1-80017, ICC), mouse monoclonal anti-acetylated K40 (Santa Cruz  
571 Biotechnology, 6-11B1 Cat#sc-23950, WB and ICC), against tubulin: mouse monoclonal anti-  
572 glutamylated tubulin (Adipogen, GT-335 Cat#AG-20B-0020-C100 and polyE Cat#AG-25B-  
573 0030-C050, WB). Labeling of actin was performed with phalloidin-Atto 390 (Sigma-Aldrich,  
574 Cat#50556, ICC) or phalloidin-TRITC (Sigma-Aldrich, Cat#P1951, ICC). Secondary antibodies  
575 conjugated with HRP were used for WB (Dako Agilent). For ICC application, and for WB  
576 application when indicated in figures, the following fluorophores conjugated to secondary  
577 antibodies were used: DYLIGHT405, AlexaFluor405, AlexaFluor488 and AlexaFluor594  
578 (Jackson, Immunoresearch) and AlexaFluor 647 (Invitrogen).

579

580 **U2OS cell lines stably co-expressing mCherry-H2B and Sept9-GFP constructs**

581 U2OS and HeLa cell lines stably expressing mCherry-H2B and a Sept9\_X-GFP construct were  
582 generated by co-transfecting the plasmid pBabeD hygro mCherry-Histone H2B (a kind gift from  
583 Christophe Lachaud, CRCM, Marseille, France) with hygromycin B resistance and one of the  
584 plasmids encoding for different Sept9 isoforms and mutants-GFP constructs, with geneticin  
585 resistance. U2OS cells were nucleo-transfected (Amaxa nucleofector program U2OS X-001,  
586 Lonza) with Amaxa kit V. Three days after transfection, co-expressing cells were selected with  
587 hygromycin B (Invitrogen, Cat#10687-010) and geneticin (Gibco, Cat#10131-027) at 0.5 mg/mL  
588 each. GFP and mCherry fluorescence positive cells were sorted by flow cytometry. Sorted cell  
589 populations were cultured in supplemented DMEM in the presence of 0.5 mg/mL of antibiotics.  
590 After three passages, cell line stocks were stored in liquid nitrogen.

591

592 **Micropatterning of U2OS cells**

593  $6 \times 10^3$  U2OS cells KD for Sept7 or Sept9 or U2OS cells stably co-expressing mCherry-H2B and  
594 Sept9-GFP constructs were seeded in each well formed by the assembly of a 35 mm collagen  
595 coated coverslip with H-shaped medium size adhesive micropatterns (Cytoo, Cat#10-008-00-18)  
596 and a magnetic four-well chamber (Cytoo, Cat#30-011) following manufacturer instructions.  
597 Coverslips were fixed with 4% formaldehyde and processed for ICC as previously described<sup>40</sup>.

598 Distance measurements were performed using the Graphics line tool in Zen blue software as  
599 described in more details in Fig. 8c legend.

### 600 **SDS-PAGE and Western blotting**

601 Total protein extraction from cells in culture by scraping the cells off in NP-40 lysis buffer,  
602 separation of proteins by SDS-PAGE using NuPAGE 4-12 % gradient Bis-Tris gels (Invitrogen,  
603 Cat#NP0322BOX) and MOPS SDS running buffer (Invitrogen, Cat#NP0001-02) and Western  
604 blotting of separated proteins on nitrocellulose were performed as described previously<sup>40</sup>.

605

### 606 **Separation of septin complexes by native gel electrophoresis and detection**

607 Native cellular protein extraction was carried out as published by Sellin et al.<sup>68</sup>. Briefly, proteins  
608 from cells at 80% confluence in one 100 mm petri dish were extracted in 40  $\mu$ l of native lysis  
609 buffer (80 mM PIPES pH 6.9, 2 mM MgCl<sub>2</sub>, 4 mM EGTA, 0.2% saponin and protease inhibitor  
610 cocktail (Roche, Cat#04693159001); the extract was incubated for 10 min on ice and centrifuged  
611 and the supernatant was supplemented with 0.45 M sodium chloride, incubated on ice,  
612 centrifuged, concentrated and exchanged twice with phosphate buffer (pH 7.5, 0.45 M NaCl, 1  
613 mM EGTA and protease inhibitors) on an Amicon 30 kDa cut off concentrator (Merck, Cat#  
614 UFC 503096). Protein concentration was determined using a BCA protein assay (Thermo  
615 Scientific, Cat#23223 and 23224), glycerol was added at 1:1 (vol:vol), and extracts stored at -  
616 20°C until use. Native PAGE was performed on 4-16% NativePAGE Novex Bis-Tris  
617 polyacrylamide gels (Thermo Scientific, Cat#BN1002BOX) following instructions from the  
618 manufacturer. Briefly, native protein extracts were mixed with 4x sample buffer (Thermo  
619 Scientific, Cat#BN2003) and water (final sample buffer 1x, and about 150 mM NaCl). Eight  $\mu$ g  
620 of proteins were loaded per lane. Unstained native protein molecular weight standards were used  
621 (Thermo Scientific, Cat#LC0725) and stained with Coomassie blue during electrophoresis.  
622 Protein complexes were transferred overnight on a PVDF membrane under 20 V constant  
623 voltage. The membrane was partially destained with 25% MeOH and 10% acetic acid, positions  
624 of native protein molecular weight standards were marked, and the membrane was placed briefly  
625 in MeOH for complete destaining. The membrane was processed for Western blot detection  
626 following the protocol used for nitrocellulose membranes described previously<sup>40</sup>.

627

### 628 **Immunocytochemistry**

629 Multiplex immunocytochemistry was carried out on cells cultured on collagen coated coverslips  
630 followed by 4% formaldehyde fixation as described previously<sup>40</sup>. Images were acquired on a  
631 Zeiss structured light ApoTome microscope equipped with a 63x/1.4 Plan Apochromat objective  
632 and an AxioCam MRc5 camera using AxioVision software or a Zeiss LSM880 META confocal  
633 microscope equipped with a 63x/1.46 Plan Apochromat objective and a GaAsP detector using  
634 Zen software.

635

636 **Co-localization of septins with microtubules and with stress fibers.** Individual cells were  
637 examined by ICC for co-localization of septins with total  $\alpha$ -tubulin, acetylated K40  $\alpha$ -tubulin and  
638 F-actin, from top to bottom. Cells were counted as positive for co-localization of septins with  
639 microtubules or with F-actin when septin fluorescence signal was co-aligned with microtubules  
640 and/or acetylated microtubules or with ventral stress fibers, respectively. The percentage of cells  
641 positive for both septin-microtubule and septin-stress fibers co-localization, only positive for  
642 septin-stress fibers co-localization and only positive for septin-microtubule co-localization were

643 designated in graphs as Microtubule+Actin, Actin, and Microtubule, respectively. The extent of  
644 the co-localizations in each cell was not considered.

645

### 646 **Quantification of acetylated microtubules in cells**

647 The fluorescence surface corresponding to acetylated microtubules in individual cells was  
648 determined using the ImageJ 1.48v software<sup>69</sup>: the fluorescence image of acetylated microtubules  
649 was converted in 8-bits, adjusted manually with the threshold function for black and white levels  
650 to maximally remove black pixels unrelated to acetylated microtubules, the actin image was  
651 synchronized with the acetylated microtubule image (Synchronize Windows tool) and used to  
652 delimit the ROI corresponding to the entire cell surface with the freehand selection tool, and  
653 finally the image was analysed using the measure function to obtain the percentage of surface area  
654 represented by the remaining black pixels corresponding to acetylated microtubule.

655

### 656 **Production and purification of recombinant human septin complexes**

657 Human septin hexameric and octameric complexes with either Sept9\_i1 or Sept9\_i3 were  
658 produced, purified and analyzed as detailed in Iv et al<sup>12</sup>. No difference in apparent MW was  
659 observed between recombinant septin octamers or hexamers and those extracted from cells after  
660 native gel separation and WB (Supplementary Fig. 1b, c).

661

### 662 **Septin/microtubule reconstitution and TIRF imaging**

663 GMPCPP-stabilized microtubule seeds serving as a nucleation site for dynamic microtubules  
664 were prepared using an established double-cycle method<sup>70</sup>. Briefly, a ~22  $\mu$ M mixture of tubulin  
665 (~11  $\mu$ M tubulin dimers) in MRB80 (80 mM PIPES pH 6.8, 4 mM MgCl<sub>2</sub>, 1 mM EGTA),  
666 composed of 75% unmodified tubulin dimers (Cytoskeleton, Inc., Ct#T240), 15% rhodamine-  
667 labeled tubulin dimers (Cytoskeleton, Inc., Cat#TL590M) and 10% biotin-modified tubulin  
668 dimers (Cytoskeleton, Inc., Cat#T333P), was spun down using an Airfuge® Air-driven  
669 ultracentrifuge (Beckman Coulter Inc., Brea, California, USA) for 5 minutes at 30 psi with a cold  
670 rotor. Then, the mixture was complemented with 1 mM GMPCPP from a 10 mM stock solution,  
671 thus diluting the tubulin to 20  $\mu$ M. This mixture was incubated at 37°C for 30 minutes to  
672 polymerize tubulin, and immediately airfuged for 5 minutes at 30 psi with the rotor at room  
673 temperature to pellet GMPCPP-stabilized microtubules. Afterwards, the supernatant was  
674 discarded and the pellet was resuspended in warm MRB80 to a final tubulin concentration of 20  
675  $\mu$ M, considering an 80% recovery of the tubulin. The mixture was incubated on ice for 20  
676 minutes to depolymerize the microtubules. Subsequently, it was complemented with 1 mM  
677 GMPCPP, incubated at 37°C for 30 minutes to repolymerize the microtubules, and airfuged for 5  
678 minutes at 30 psi with a warm rotor. The pellet, containing GMPCPP-stabilized microtubule  
679 seeds, was resuspended in warm MRB80 supplemented with 10% glycerol, snap-frozen, and  
680 kept at -80°C until use.

681 Nr. 1 Menzel coverslips (Thermo Fisher scientific, product number 11961988) and glass slides  
682 (Thermo Fisher scientific, product number 11879022) were cleaned in base piranha solution (5%  
683 hydrogen peroxide, 5% ammonium hydroxide) at 70°C for 10 minutes, washed extensively by  
684 rinsing with Milli-Q water and stored in Milli-Q water for up to 5 days. Just before use, a  
685 coverslip and a glass slide were blow dried with a stream of N<sub>2</sub> gas. Flow channels were  
686 prepared by placing parallel 2x20 mm parafilm strips spaced by 2-3 mm between the glass slide  
687 and the coverslip. The parafilm was melted by placing the chambers on a hotplate at 120°C.  
688 After cooling down, the chambers were passivated by incubation with 0.2 mg/mL Poly(L-

689 lysine)-graft-biotinylated PEG (SuSoS, product number CHF560.00) in MRB80, 0.2 mg/mL  
690 neutravidin in MRB80, 0.5mg/mL  $\kappa$ -casein in MRB80, and 1 wt% Pluronic F-127 in MRB80, in  
691 that order and without intervening washing steps. The channels were washed with three channel  
692 volumes (~30  $\mu$ L) of MRB80 at the end of the passivation process. Then the channels were  
693 incubated for 10 minutes with an aliquot of GMPCPP-stabilized seeds that was quickly thawed at  
694 37°C, allowing the microtubule seeds to bind to the surface via biotin-neutravidin interactions.  
695 Microtubule polymerization was induced by immediately flushing into the channel 20  $\mu$ M  
696 tubulin (3% rhodamine-labeled tubulin) in a 5:1 volume ratio of MRB80:septin buffer  
697 complemented with 0.5 mg/mL  $\kappa$ -casein to prevent unspecific interactions, 0.1% methylcellulose  
698 as a crowding agent, 1 mM ATP, 1 mM GTP and an oxygen scavenging system composed of 50  
699 mM glucose, 200  $\mu$ g/ml catalase, 400  $\mu$ g/ml glucose-oxidase, and 4 mM DTT. A mixture of 90%  
700 unlabelled and 10% msGFP-labeled septin hetero-hexamers or hetero-octamers (containing  
701 either SEPT9\_i1 or Sept9\_i3) were added to the previous mix at different concentrations in the  
702 range of 10 to 300 nM.

703 The samples were immediately imaged using a Nikon Ti2-E microscope complemented with a  
704 Gataca iLAS2 azimuthal TIRF illumination system heated to 30°C using an Okolab incubator  
705 system. The sample was illuminated with 488-nm and 561-nm lasers (Gataca laser combiner  
706 iLAS2) to visualize the septin and the tubulin signals, respectively. To achieve fast imaging, the  
707 fluorescence signal was split with a Cairn Research Optosplit II ByPass containing a Chroma ZT  
708 543 rdc dichroic mirror and filtered with either a 525/50 or a 600/50 chroma bandpass filter. The  
709 images were recorded with a Andor iXon Ultra 897 EM-CCD camera using an exposure time of  
710 75 ms, for 10-20 minutes with a frame rate of 1 frame/second.

711 Microtubule dynamics were analysed by kymograph analysis<sup>71</sup>. Kymographs were built with the  
712 reslice tool in FIJI<sup>69</sup> on a manually drawn line that went from the beginning of the microtubule  
713 seed to the tip of the microtubule in its maximum length. In the kymographs, we can observe the  
714 positions of the microtubule tips over time. The analysis was only done on the plus ends of the  
715 microtubules, which can be distinguished from the minus ends via the longer final length and  
716 higher growth velocity of the former. Growth and shortening rates were obtained as the slopes of  
717 manually fitted straight lines on the growing or shortening contour phases, determined by manual  
718 inspection, of the microtubule plus ends. The catastrophe rate was calculated as the inverse of the  
719 time that a microtubule spends growing.

720

## 721 **Statistical analysis**

722 Unless indicated otherwise, statistical analysis was performed using GraphPad Prism software  
723 and unpaired two-tailed t-test with Welch correction for cell related data or using the function  
724 `compare_means` from the package `ggpubr` from R and two-tailed t-test with Benjamini &  
725 Hochberg p-value correction (<https://rpkgs.datanovia.com/ggpubr/index.html>) for the *in vitro*  
726 data related to microtubule dynamics.

727

728

729

730

731

732

733

734

735 **References**

736

- 737 1 Janke, C. & Magiera, M. M. The tubulin code and its role in controlling microtubule  
738 properties and functions. *Nat Rev Mol Cell Biol* **21**, 307-326, doi:10.1038/s41580-020-  
739 0214-3 (2020).
- 740 2 Carlton, J. G., Jones, H. & Eggert, U. S. Membrane and organelle dynamics during cell  
741 division. *Nat Rev Mol Cell Biol* **21**, 151-166, doi:10.1038/s41580-019-0208-1 (2020).
- 742 3 Maninova, M., Caslavsky, J. & Vomastek, T. The assembly and function of perinuclear  
743 actin cap in migrating cells. *Protoplasma* **254**, 1207-1218, doi:10.1007/s00709-017-  
744 1077-0 (2017).
- 745 4 Sneider, A., Hah, J., Wirtz, D. & Kim, D. H. Recapitulation of molecular regulators of  
746 nuclear motion during cell migration. *Cell Adh Migr* **13**, 50-62,  
747 doi:10.1080/19336918.2018.1506654 (2019).
- 748 5 Dogterom, M. & Koenderink, G. H. Actin-microtubule crosstalk in cell biology. *Nat Rev*  
749 *Mol Cell Biol* **20**, 38-54, doi:10.1038/s41580-018-0067-1 (2019).
- 750 6 Woods, B. L. & Gladfelter, A. S. The state of the septin cytoskeleton from assembly to  
751 function. *Curr Opin Cell Biol* **68**, 105-112, doi:10.1016/j.ceb.2020.10.007 (2020).
- 752 7 Valadares, N. F., d' Muniz Pereira, H., Ulian Araujo, A. P. & Garratt, R. C. Septin  
753 structure and filament assembly. *Biophys Rev* **9**, 481-500, doi:10.1007/s12551-017-0320-  
754 4 (2017).
- 755 8 Bertin, A. *et al.* Three-dimensional ultrastructure of the septin filament network in  
756 *Saccharomyces cerevisiae*. *Mol Biol Cell* **23**, 423-432, doi:10.1091/mbc.E11-10-0850  
757 (2012).
- 758 9 DeRose, B. T. *et al.* Production and analysis of a mammalian septin hetero-octamer  
759 complex. *Cytoskeleton (Hoboken)* **77**, 485-499, doi:10.1002/cm.21643 (2020).
- 760 10 Soroor, F. *et al.* Revised subunit order of mammalian septin complexes explains their in  
761 vitro polymerization properties. *Mol Biol Cell* **32**, 289-300, doi:10.1091/mbc.E20-06-  
762 0398 (2021).
- 763 11 Szuba, A. *et al.* Membrane binding controls ordered self-assembly of animal septins.  
764 *bioRxiv*, 2020.2009.2022.307918, doi:10.1101/2020.09.22.307918 (2020).
- 765 12 Iv, F. *et al.* Insights into animal septins using recombinant human septin octamers with  
766 distinct SEPT9 isoforms. *bioRxiv*, 2021.2001.2021.427698,  
767 doi:10.1101/2021.01.21.427698 (2021).
- 768 13 Ong, K., Wloka, C., Okada, S., Svitkina, T. & Bi, E. Architecture and dynamic  
769 remodelling of the septin cytoskeleton during the cell cycle. *Nat Commun* **5**, 5698,  
770 doi:10.1038/ncomms6698 (2014).
- 771 14 Fung, K. Y., Dai, L. & Trimble, W. S. Cell and molecular biology of septins. *Int Rev Cell*  
772 *Mol Biol* **310**, 289-339, doi:10.1016/B978-0-12-800180-6.00007-4 (2014).
- 773 15 Marquardt, J., Chen, X. & Bi, E. Architecture, remodeling, and functions of the septin  
774 cytoskeleton. *Cytoskeleton (Hoboken)* **76**, 7-14, doi:10.1002/cm.21475 (2019).
- 775 16 Mostowy, S. & Cossart, P. Septins: the fourth component of the cytoskeleton. *Nat Rev*  
776 *Mol Cell Biol* **13**, 183-194, doi:10.1038/nrm3284 (2012).
- 777 17 Renshaw, M. J., Liu, J., Lavoie, B. D. & Wilde, A. Anillin-dependent organization of  
778 septin filaments promotes intercellular bridge elongation and Chmp4B targeting to the  
779 abscission site. *Open Biol* **4**, 130190, doi:10.1098/rsob.130190 (2014).

- 780 18 Oegema, K., Savoian, M. S., Mitchison, T. J. & Field, C. M. Functional analysis of a  
781 human homologue of the Drosophila actin binding protein anillin suggests a role in  
782 cytokinesis. *J Cell Biol* **150**, 539-552, doi:10.1083/jcb.150.3.539 (2000).
- 783 19 Straight, A. F. & Field, C. M. Microtubules, membranes and cytokinesis. *Curr Biol* **10**,  
784 R760-770, doi:10.1016/s0960-9822(00)00746-6 (2000).
- 785 20 Verma, V. & Maresca, T. J. Microtubule plus-ends act as physical signaling hubs to  
786 activate RhoA during cytokinesis. *Elife* **8**, doi:10.7554/eLife.38968 (2019).
- 787 21 Estey, M. P., Di Ciano-Oliveira, C., Froese, C. D., Bejide, M. T. & Trimble, W. S.  
788 Distinct roles of septins in cytokinesis: SEPT9 mediates midbody abscission. *J Cell Biol*  
789 **191**, 741-749, doi:10.1083/jcb.201006031 (2010).
- 790 22 Kim, M. S., Froese, C. D., Estey, M. P. & Trimble, W. S. SEPT9 occupies the terminal  
791 positions in septin octamers and mediates polymerization-dependent functions in  
792 abscission. *J Cell Biol* **195**, 815-826, doi:10.1083/jcb.201106131 (2011).
- 793 23 Kinoshita, M. *et al.* Nedd5, a mammalian septin, is a novel cytoskeletal component  
794 interacting with actin-based structures. *Genes Dev* **11**, 1535-1547,  
795 doi:10.1101/gad.11.12.1535 (1997).
- 796 24 Surka, M. C., Tsang, C. W. & Trimble, W. S. The mammalian septin MSF localizes with  
797 microtubules and is required for completion of cytokinesis. *Mol Biol Cell* **13**, 3532-3545,  
798 doi:10.1091/mbc.e02-01-0042 (2002).
- 799 25 Addi, C., Bai, J. & Echard, A. Actin, microtubule, septin and ESCRT filament  
800 remodeling during late steps of cytokinesis. *Curr Opin Cell Biol* **50**, 27-34,  
801 doi:10.1016/j.ceb.2018.01.007 (2018).
- 802 26 Yadav, S. *et al.* TAOK2 Kinase Mediates PSD95 Stability and Dendritic Spine  
803 Maturation through Septin7 Phosphorylation. *Neuron* **93**, 379-393,  
804 doi:10.1016/j.neuron.2016.12.006 (2017).
- 805 27 Tada, T. *et al.* Role of Septin cytoskeleton in spine morphogenesis and dendrite  
806 development in neurons. *Curr Biol* **17**, 1752-1758, doi:10.1016/j.cub.2007.09.039  
807 (2007).
- 808 28 Nolke, T. *et al.* Septins guide microtubule protrusions induced by actin-depolymerizing  
809 toxins like Clostridium difficile transferase (CDT). *Proc Natl Acad Sci U S A* **113**, 7870-  
810 7875, doi:10.1073/pnas.1522717113 (2016).
- 811 29 Ostevold, K. *et al.* Septin remodeling is essential for the formation of cell membrane  
812 protrusions (microtentacles) in detached tumor cells. *Oncotarget* **8**, 76686-76698,  
813 doi:10.18632/oncotarget.20805 (2017).
- 814 30 Spiliotis, E. T. Regulation of microtubule organization and functions by septin GTPases.  
815 *Cytoskeleton (Hoboken)* **67**, 339-345, doi:10.1002/cm.20448 (2010).
- 816 31 Sirajuddin, M. *et al.* Structural insight into filament formation by mammalian septins.  
817 *Nature* **449**, 311-315, doi:10.1038/nature06052 (2007).
- 818 32 Sellin, M. E., Stenmark, S. & Gullberg, M. Mammalian SEPT9 isoforms direct  
819 microtubule-dependent arrangements of septin core heteromers. *Mol Biol Cell* **23**, 4242-  
820 4255, doi:10.1091/mbc.E12-06-0486  
821 mbc.E12-06-0486 [pii] (2012).
- 822 33 Mendonca, D. C. *et al.* A revised order of subunits in mammalian septin complexes.  
823 *Cytoskeleton (Hoboken)* **76**, 457-466, doi:10.1002/cm.21569 (2019).
- 824 34 Connolly, D., Abdesselam, I., Verdier-Pinard, P. & Montagna, C. Septin roles in  
825 tumorigenesis. *Biol Chem* **392**, 725-738, doi:10.1515/BC.2011.073 (2011).

- 826 35 Kuhlenbaumer, G. *et al.* Mutations in SEPT9 cause hereditary neuralgic amyotrophy. *Nat*  
827 *Genet* **37**, 1044-1046, doi:10.1038/ng1649 (2005).
- 828 36 Hannibal, M. C. *et al.* SEPT9 gene sequencing analysis reveals recurrent mutations in  
829 hereditary neuralgic amyotrophy. *Neurology* **72**, 1755-1759,  
830 doi:10.1212/WNL.0b013e3181a609e3 (2009).
- 831 37 Collie, A. M. *et al.* Non-recurrent SEPT9 duplications cause hereditary neuralgic  
832 amyotrophy. *J Med Genet* **47**, 601-607, doi:10.1136/jmg.2009.072348 (2010).
- 833 38 McIlhatton, M. A. *et al.* Genomic organization, complex splicing pattern and expression  
834 of a human septin gene on chromosome 17q25.3. *Oncogene* **20**, 5930-5939,  
835 doi:10.1038/sj.onc.1204752 (2001).
- 836 39 Connolly, D. *et al.* Septin 9 isoform expression, localization and epigenetic changes  
837 during human and mouse breast cancer progression. *Breast Cancer Res* **13**, R76,  
838 doi:10.1186/bcr2924 (2011).
- 839 40 Verdier-Pinard, P. *et al.* Septin 9<sub>i2</sub> is downregulated in tumors, impairs cancer cell  
840 migration and alters subnuclear actin filaments. *Sci Rep* **7**, 44976, doi:10.1038/srep44976  
841 (2017).
- 842 41 Bai, X. *et al.* Novel septin 9 repeat motifs altered in neuralgic amyotrophy bind and  
843 bundle microtubules. *J Cell Biol* **203**, 895-905, doi:10.1083/jcb.201308068 (2013).
- 844 42 Nagata, K. *et al.* Filament formation of MSF-A, a mammalian septin, in human  
845 mammary epithelial cells depends on interactions with microtubules. *J Biol Chem* **278**,  
846 18538-18543, doi:10.1074/jbc.M205246200 (2003).
- 847 43 Buschmann, H. *et al.* Microtubule-associated AIR9 recognizes the cortical division site at  
848 preprophase and cell-plate insertion. *Curr Biol* **16**, 1938-1943,  
849 doi:10.1016/j.cub.2006.08.028 (2006).
- 850 44 Bertin, A. *et al.* Phosphatidylinositol-4,5-bisphosphate promotes budding yeast septin  
851 filament assembly and organization. *J Mol Biol* **404**, 711-731,  
852 doi:10.1016/j.jmb.2010.10.002 (2010).
- 853 45 Kim, M. S., Froese, C. D., Xie, H. & Trimble, W. S. Uncovering principles that control  
854 septin-septin interactions. *J Biol Chem* **287**, 30406-30413, doi:10.1074/jbc.M112.387464  
855 (2012).
- 856 46 Kellogg, E. H. *et al.* Near-atomic model of microtubule-tau interactions. *Science* **360**,  
857 1242-1246, doi:10.1126/science.aat1780 (2018).
- 858 47 Shigematsu, H. *et al.* Structural insight into microtubule stabilization and kinesin  
859 inhibition by Tau family MAPs. *J Cell Biol* **217**, 4155-4163, doi:10.1083/jcb.201711182  
860 (2018).
- 861 48 Spiliotis, E. T., Hunt, S. J., Hu, Q., Kinoshita, M. & Nelson, W. J. Epithelial polarity  
862 requires septin coupling of vesicle transport to polyglutamylated microtubules. *J Cell*  
863 *Biol* **180**, 295-303, doi:10.1083/jcb.200710039 (2008).
- 864 49 Froidevaux-Klipfel, L. *et al.* Septin cooperation with tubulin polyglutamylation  
865 contributes to cancer cell adaptation to taxanes. *Oncotarget* **6**, 36063-36080,  
866 doi:10.18632/oncotarget.5373 (2015).
- 867 50 Janke, C. & Montagnac, G. Causes and Consequences of Microtubule Acetylation. *Curr*  
868 *Biol* **27**, R1287-R1292, doi:10.1016/j.cub.2017.10.044 (2017).
- 869 51 Hein, M. Y. *et al.* A human interactome in three quantitative dimensions organized by  
870 stoichiometries and abundances. *Cell* **163**, 712-723, doi:10.1016/j.cell.2015.09.053  
871 (2015).

- 872 52 Targa, B. *et al.* Septin filament coalignment with microtubules depends on SEPT9\_i1 and  
873 tubulin polyglutamylation, and is an early feature of acquired cell resistance to paclitaxel.  
874 *Cell Death Dis* **10**, 54, doi:10.1038/s41419-019-1318-6 (2019).
- 875 53 Farrugia, A. J. *et al.* CDC42EP5/BORG3 modulates SEPT9 to promote actomyosin  
876 function, migration, and invasion. *J Cell Biol* **219**, doi:10.1083/jcb.201912159 (2020).
- 877 54 They, M., Pepin, A., Dressaire, E., Chen, Y. & Bornens, M. Cell distribution of stress  
878 fibres in response to the geometry of the adhesive environment. *Cell Motil Cytoskeleton*  
879 **63**, 341-355, doi:10.1002/cm.20126 (2006).
- 880 55 Serrano, L., Montejo de Garcini, E., Hernandez, M. A. & Avila, J. Localization of the  
881 tubulin binding site for tau protein. *Eur J Biochem* **153**, 595-600, doi:10.1111/j.1432-  
882 1033.1985.tb09342.x (1985).
- 883 56 Nakos, K., Rosenberg, M. & Spiliotis, E. T. Regulation of microtubule plus end  
884 dynamics by septin 9. *Cytoskeleton (Hoboken)* **76**, 83-91, doi:10.1002/cm.21488 (2019).
- 885 57 Karasmanis, E. P. *et al.* Polarity of Neuronal Membrane Traffic Requires Sorting of  
886 Kinesin Motor Cargo during Entry into Dendrites by a Microtubule-Associated Septin.  
887 *Dev Cell* **46**, 518-524, doi:10.1016/j.devcel.2018.08.004 (2018).
- 888 58 Nakos, K., Radler, M. R. & Spiliotis, E. T. Septin 2/6/7 complexes tune microtubule  
889 plus-end growth and EB1 binding in a concentration- and filament-dependent manner.  
890 *Mol Biol Cell* **30**, 2913-2928, doi:10.1091/mbc.E19-07-0362 (2019).
- 891 59 Bowen, J. R., Hwang, D., Bai, X., Roy, D. & Spiliotis, E. T. Septin GTPases spatially  
892 guide microtubule organization and plus end dynamics in polarizing epithelia. *J Cell Biol*  
893 **194**, 187-197, doi:10.1083/jcb.201102076 (2011).
- 894 60 Ghossoub, R. *et al.* Septins 2, 7 and 9 and MAP4 colocalize along the axoneme in the  
895 primary cilium and control ciliary length. *J Cell Sci* **126**, 2583-2594,  
896 doi:10.1242/jcs.111377 (2013).
- 897 61 Hu, J. *et al.* Septin-driven coordination of actin and microtubule remodeling regulates the  
898 collateral branching of axons. *Curr Biol* **22**, 1109-1115, doi:10.1016/j.cub.2012.04.019  
899 (2012).
- 900 62 Zacharias, D. A., Violin, J. D., Newton, A. C. & Tsien, R. Y. Partitioning of lipid-  
901 modified monomeric GFPs into membrane microdomains of live cells. *Science* **296**, 913-  
902 916, doi:10.1126/science.1068539 (2002).
- 903 63 Costantini, L. M., Fossati, M., Francolini, M. & Snapp, E. L. Assessing the tendency of  
904 fluorescent proteins to oligomerize under physiologic conditions. *Traffic* **13**, 643-649,  
905 doi:10.1111/j.1600-0854.2012.01336.x (2012).
- 906 64 Cranfill, P. J. *et al.* Quantitative assessment of fluorescent proteins. *Nature methods* **13**,  
907 557-562, doi:10.1038/nmeth.3891 (2016).
- 908 65 Pedelacq, J. D., Cabantous, S., Tran, T., Terwilliger, T. C. & Waldo, G. S. Engineering  
909 and characterization of a superfolder green fluorescent protein. *Nature biotechnology* **24**,  
910 79-88, doi:10.1038/nbt1172 (2006).
- 911 66 Shaner, N. C. *et al.* Improving the photostability of bright monomeric orange and red  
912 fluorescent proteins. *Nature methods* **5**, 545-551, doi:10.1038/nmeth.1209 (2008).
- 913 67 Shida, T., Cueva, J. G., Xu, Z., Goodman, M. B. & Nachury, M. V. The major alpha-  
914 tubulin K40 acetyltransferase alphaTAT1 promotes rapid ciliogenesis and efficient  
915 mechanosensation. *Proc Natl Acad Sci U S A* **107**, 21517-21522,  
916 doi:10.1073/pnas.1013728107 (2010).

- 917 68 Sellin, M. E., Stenmark, S. & Gullberg, M. Cell type-specific expression of SEPT3-  
918 homology subgroup members controls the subunit number of heteromeric septin  
919 complexes. *Mol Biol Cell* **25**, 1594-1607, doi:10.1091/mbc.E13-09-0553 (2014).  
920 69 Schneider, C. A., Rasband, W. S. & Eliceiri, K. W. NIH Image to ImageJ: 25 years of  
921 image analysis. *Nat Methods* **9**, 671-675, doi:10.1038/nmeth.2089 (2012).  
922 70 Gell, C. *et al.* Microtubule dynamics reconstituted in vitro and imaged by single-  
923 molecule fluorescence microscopy. *Methods Cell Biol* **95**, 221-245, doi:10.1016/S0091-  
924 679X(10)95013-9 (2010).  
925 71 Bieling, P. *et al.* Reconstitution of a microtubule plus-end tracking system in vitro.  
926 *Nature* **450**, 1100-1105, doi:10.1038/nature06386 (2007).  
927  
928  
929

### 930 **Acknowledgements**

931 This research received funding from the Agence Nationale pour la Recherche (ANR grant ANR-  
932 17-CE13-0014; SEPTIMORF) (to M.M. and P. V-P.). We thank Jeffrey den Haan (TU Delft,  
933 The Netherlands) for help with protein purification. This work was further financially supported  
934 by the Netherlands Organization for Scientific Research (NWO/OCW) through the ‘BaSyC-  
935 Building a Synthetic Cell’ Gravitation grant (024.003.019) (to G.K.).  
936

### 937 **Authors contributions**

938 J. Fialová, F. Iv, A. Llewellyn, M. Belhabib, M. Gomes, Y. Liu, K. Asano, D. Salaün:  
939 investigation; M. Kuzmić, G. Castro Linares investigation, writing – review & editing; T.  
940 Tachibana, supervision, resources, funding acquisition; G. H. Koenderink, A. Badache,  
941 conceptualization, funding acquisition, supervision, writing – review & editing; M. Mavrakis,  
942 investigation, conceptualization, methodology, funding acquisition, supervision, writing – review  
943 & editing; P. Verdier-Pinard, investigation, conceptualization, methodology, funding acquisition,  
944 supervision, writing – original draft, writing – review & editing.  
945  
946  
947  
948  
949  
950  
951  
952  
953  
954  
955  
956  
957  
958  
959  
960  
961  
962  
963

964 **Figure legends**

965 **Fig 1. Sept9 expression, incorporation in octamers and localization in human cell lines. a**  
966 Western blots of total protein extracts from U2OS, HeLa, RPE1 and SKBr3 cells probed with  
967 antibodies against septins and tubulin. **b** Native extracts from the same cell lines were analyzed  
968 by Western blotting for their content in both septin hexamers and octamers using antibodies  
969 against constitutively required Sept7 and ubiquitously expressed Sept8; septin octamers were  
970 also specifically labeled with a pan Sept9 antibody. Relative content in septin octamers and  
971 hexamers in each cell line based on three independent Sept7 WB is presented below the blots  
972 (mean  $\pm$  SEM). **c** and **d** Cellular localization by immunocytochemistry of Sept9 in the same cell  
973 lines, during interphase and cytokinesis; in **c**, the percentages of cells displaying both co-  
974 localization of Sept9 with microtubules and co-localization with stress fibers (Microtubule +  
975 Actin) or only stress fibers (Actin) were determined from three independent experiments based  
976 on a total of 90 cells (30 cells per experiment). Unpaired, two-tailed t-test with Welch's  
977 correction, \*\*  $p < 0.01$ , \*\*\*  $p < 0.0005$ , Microtubule and Actin localization vs in SKBr3; in **d**,  
978 white scale bars correspond to 5  $\mu\text{m}$ , insets are two-fold zoomed regions framed by a white  
979 square in the corresponding original images. **e** RPE1 cells were starved for 24 h and  
980 immunofluorescence was performed as in **c** and **d**; white scale bars correspond to 5  $\mu\text{m}$ , a three-  
981 fold zoom of a region framed in white containing a primary cilium is presented below the  
982 original images.

983  
984 **Fig. 2. Identification of the microtubule binding domain in Sept9\_i1. a** Top part: human  
985 Sept9\_i1 specific amino-acid N-terminal sequence (1-24) was aligned with the homologous plant  
986 *A. thaliana* AIR9 sequences (173-205 and 46-78) contained in the AIR-9 microtubule binding  
987 domain (MBD)<sup>43</sup>; bottom part: Sept9\_i1 and AIR9 sequences in top part were aligned with  
988 sequences of tandem repeats involved in the binding of human structural MAPs (Tau, MAP4 and  
989 MAP2) to microtubules (ex: Tau 4R isoform positions of repeats are R1<sub>242-273</sub>, R2<sub>274-304</sub>, R3<sub>305-335</sub>  
990 and R4<sub>336-367</sub>). Alignments were adjusted by introducing gaps and similar aa residues were  
991 manually coded, orange: common to AIR9 and MAPs; yellow: common to Sept9\_i1, AIR9 and  
992 MAPs; light green: common to Sept9\_i1 and MAPs; dark green: common to MAPs; dark blue:  
993 common to Sept9\_i1 and AIR9; light blue: common to AIR9 repeats. Important serine residues  
994 and hydrophobic residues of MAPs involved in MAP repeat-microtubule lattice interactions are  
995 framed in red and marked with a red asterisk, respectively. Horizontal blue line and red line  
996 indicate, respectively, the position of Tau R2 repeat and Tau R1/MAP4 R1 repeat modeled based  
997 on the cryo-EM structural determination of MAP repeated sequences bound on microtubules *in*  
998 *vitro*<sup>46,47</sup>. **b** Schematic representation of the Sept9\_i1 mutants in the predicted MBD tagged with  
999 GFP at their C-terminus. **c, d** Co-localization of each Sept9 construct transfected in U2OS cells  
1000 with microtubules or stress fibers during interphase was analyzed as described in Fig. 1 legend.  
1001 Unpaired, two-tailed t-test with Welch's correction, \*\*  $p < 0.01$ , Microtubule and Actin  
1002 localization vs Sept9\_i1 wt; white scale bars 5  $\mu\text{m}$ , insets: three-fold zooms. **e** Schematic  
1003 representation of Sept9 isoforms (Sept9\_i1, \_i5 and \_i3), of the chimeric construct fusing the  
1004 Sept9\_i1 MBD to the N-terminus of Sept9\_i5 (Sept9\_i1-i5) and of Sept9\_i1 HNA mutants, all  
1005 tagged with GFP at their C-terminus. **f** Co-localization of Sept9\_i5 or \_i1-i5 or \_i3, and **g** of  
1006 Sept9 HNA point mutants with microtubules or stress fibers in U2OS transfected cells during  
1007 interphase. Unpaired, two-tailed t-test with Welch's correction, \*\*  $p < 0.01$ . **h** Images showing  
1008 co-localization of Sept9 in U2OS cells transfected with constructs described in **e**; white scale  
1009 bars 10  $\mu\text{m}$ , insets: 1.4-fold zooms.

1010 **Fig. 3. Dependence of septin association with microtubules on the incorporation of Sept9\_i1**  
1011 **in polymerized septin octamers. a** Top, predicted septin complexes when Sept9\_i1 wt, or  
1012 Sept9\_i1 mutated on its G (G<sub>mut</sub>, blue dots) or NC interface (NC<sub>mut</sub>, yellow dot) is expressed in  
1013 cells; bottom, Western blots of native gels resolving septin complexes present in U2OS cells  
1014 expressing indicated siRNA and Sept9\_i1 wt or Sept9\_i1 interface mutants. **b** GFP-fluorescence  
1015 based co-localization of Sept9\_i1 wt or interface mutants with actin and microtubules; Sept9\_i1  
1016 wt co-localized both with microtubule and actin fibers as expected, but non-octameric septin  
1017 complexes containing an interface mutant Sept9\_i1 did not. White scale bar 10  $\mu$ m, insets: two-  
1018 fold zooms of frames region. **c** Top, predicted septin complexes when Sept2 wt or Sept2 mutated  
1019 on its NC interface (NC<sub>mut</sub>, yellow dots) is co-expressed with Sept9\_i1 in U2OS cells; bottom,  
1020 Western blots of native gels resolving septin complexes present in U2OS expressing indicated  
1021 siRNAs and septin constructs. **d** mApple and GFP-based co-localization of Sept2 and Sept9\_i1,  
1022 respectively, with actin and microtubules; expression of Sept2 NC mutant prevented normal co-  
1023 localization of octamers harboring Sept9\_i1 with acetylated microtubules and actin fibers. Insets:  
1024 individual fluorescence channel images of framed regions.

1025  
1026 **Fig. 4. Sept9\_i1 selective binding on, and stabilization of, microtubule bundles. a**  
1027 Differential co-localization of endogenous Sept7 vs MAP4 with microtubule cytoskeleton in  
1028 SKBr3 cells. **b** Differential co-localization between endogenous MAP4 and transfected  
1029 Sept9\_i1-GFP or Sept9\_i1-i5-GFP with microtubule cytoskeleton in U2OS cells. White scale  
1030 bars 5  $\mu$ m in merge images. **c** Analysis of the percent of U2OS cells KD for Sept9 and  
1031 expressing the indicated Sept9-GFP constructs, displaying either microtubule or actin or mixed  
1032 cytoskeleton co-localization with GFP during interphase, and treated either with DMSO vehicle  
1033 alone (D) or 2  $\mu$ M paclitaxel (P) or 10  $\mu$ M nocodazole (N) for 2 hrs. Results are from the  
1034 analysis on a total of 90 cells from three independent experiments based (30 cells per  
1035 experiment). Unpaired, two-tailed t-test with Welch's correction, \*\*  $p < 0.01$ , microtubule and  
1036 actin localization vs DMSO. **d** Quantification of nocodazole-resistant acetylated microtubules  
1037 (treatment as in c) in U2OS cells KD for Sept9 and expressing the indicated Sept9-GFP  
1038 constructs. Results are from the analysis of a total of 150 cells from three independent  
1039 experiments (50 cells per experiments). Unpaired, two-tailed t-test with Welch's correction, \*  
1040  $p < 0.05$ , \*\*\*  $p < 0.0005$ .

1041  
1042 **Fig. 5. Dependence of Sept9\_i1 binding to microtubules on their bundling but not on their**  
1043 **acetylation or polyglutamylation. a** Left: Western blots of total protein extracts from indicated  
1044 cell lines, probed for Sept9\_i1,  $\alpha$ -tubulin acetylation on K40, glutamylation (one or two  
1045 glutamate residues) and polyglutamylation of tubulin; as a positive control for these tubulin  
1046 posttranslational modifications, an equivalent amount of purified porcine brain tubulin (Brain  
1047 tub) was included in the last lane. Right: quantification of tubulin acetylation levels in cell lines  
1048 based on acetylated  $\alpha$ -tubulin and total  $\alpha$ -tubulin Western blots. Results are from three  
1049 independent determinations. Unpaired, two-tailed t-test with Welch's correction, \*  $p < 0.05$ , \*\*  $p <$   
1050  $0.01$ , tubulin acetylation levels vs ARPE19. **b** Left: Co-localization by immunocytochemistry of  
1051 Sept7 with microtubules and/or actin fibers in RPE1 and ARPE19 cells during interphase; white  
1052 scale bars 10  $\mu$ m, insets: two-fold zooms of framed regions. Right: quantification of this co-  
1053 localization from three independent experiments on a total of 90 cells (30 cells per experiments).  
1054 **c** Left: Co-localization by immunocytochemistry of Sept7 with microtubules bundles induced by  
1055 paclitaxel treatment (PTX) and/or with actin fibers in RPE1 and ARPE19 cells; white scale bar

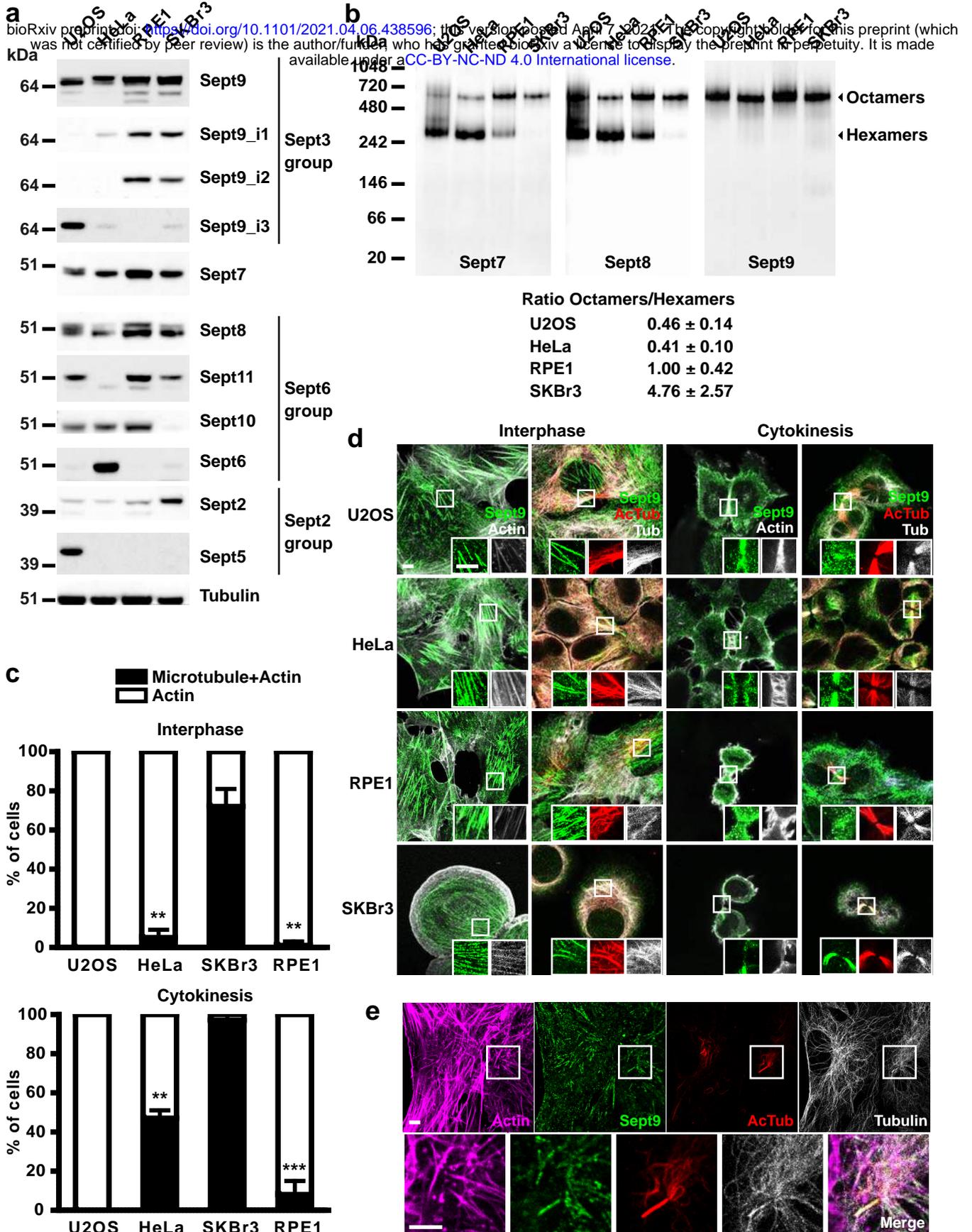
1056 10  $\mu\text{m}$ , insets: two-fold zooms of framed regions. Right: Western blots as described in **a** for total  
1057 protein extracts of cells that were treated with vehicle alone (DMSO) or PTX. **d** Left: Co-  
1058 localization by immunocytochemistry of Sept7 with microtubules bundles induced by paclitaxel  
1059 treatment (PTX) in RPE1 cells either transfected with a control siRNA (siCtrl) or a siRNA  
1060 against the  $\alpha$ -tubulin acetyl transferase 1 ( $\alpha$ TAT1); white scale bar 10  $\mu\text{m}$ . Right: Western blot of  
1061 total protein extracts from PTX treated RPE1 cells as described in the left part, showing down-  
1062 regulation of  $\alpha$ -tubulin acetylation upon  $\alpha$ TAT1 KD.  
1063

1064 **Fig. 6. Recombinant septin octamers containing Sept9\_i1 specifically bind microtubules *in***  
1065 ***vitro*.** **a** Schematic representation of the *in vitro* assay. Biotinylated GMPCPP-stabilized  
1066 microtubule seeds were immobilized on a streptavidin coated passivated glass coverslip, and free  
1067 tubulin heterodimers (10  $\mu\text{M}$ ) along with septin octamers (nM concentrations as indicated  
1068 containing 10% msfGFP-labeled septins) were added. The seeds were labelled with a higher  
1069 percentage (30%) of rhodamine-tubulin heterodimers than the free tubulin added (3-6%) to be  
1070 able to distinguish the seed from the dynamic microtubules while using the same fluorophore. **b**  
1071 Septin octamers harboring either Sept9\_i1 or \_i3 subunits (Oct\_9i1 or Oct\_9i3) were introduced  
1072 in the chamber at the indicated concentrations and their binding observed on dynamic  
1073 microtubules (examples of sporadic binding indicated by white arrow heads) and stable  
1074 microtubule seeds (examples indicated by yellow arrow heads). White scale bar 5  $\mu\text{m}$ . **c**  
1075 Examples (#1 and #2) of representative kymographs of microtubules observed as in **b** in the  
1076 presence of the minimal (10 nM) or maximal (300 nM) septin octamer concentrations. False  
1077 colors for rhodamine (Tub) and GFP (Sept2) fluorescence signals were used to optimize visually  
1078 their merged image (third image from the left of each condition). Horizontal white scale bar 5  
1079  $\mu\text{m}$ ; vertical white scale bar 50 sec.  
1080

1081 **Fig. 7. Recombinant septin octamers containing Sept9\_i1 reduce the shortening rate of**  
1082 **dynamic microtubules *in vitro*.** **a** Quantitation of microtubule dynamic parameters (growth rate,  
1083 shortening rate, and catastrophe time frequency) at increasing septin octamer concentrations.  
1084 Results are presented as box and whiskers plots superposed with individual data points including  
1085 outliers. The number of microtubules used (n) and mean value are indicated under each plot.  
1086 (grey: no septin octamers, pink: octamers with Sept9\_i1, light blue: octamers with Sept9\_i3).  
1087 Two-tailed t-test with Benjamini & Hochberg p-value correction with R, \*  $p < 0.05$ , \*\*  $p < 0.01$ ,  
1088 \*\*\*  $p < 0.001$ , \*\*\*\*  $p < 0.0001$ . Right inset graphs show median values of each parameter in the  
1089 absence of octamers (black dots) and direct comparison in presence of either octamers with  
1090 Sept9\_i1 (red dots) or octamers with Sept9\_i3 (blue dots) and corresponding interquartile ranges.  
1091 **b** Representative kymographs (rhodamine channel for tubulin) representing the effect of  
1092 recombinant septin octamers on microtubule dynamics. Such kymographs were used to calculate  
1093 the parameters values presented in **a** from individual microtubules. First kymograph on the left is  
1094 in the absence of septin octamers. Horizontal white scale bar 5  $\mu\text{m}$ ; vertical white scale bar 50  
1095 sec. **c** Snapshots at indicated times (min:sec) of a microtubule and associated septin octamers  
1096 harboring Sept9\_i1 (200 nM, Supplementary Movie 3). Yellow arrow heads point at a curved  
1097 structure on a depolymerizing microtubule (+) end. White scale bar 5  $\mu\text{m}$ .  
1098  
1099  
1100

1101 **Fig. 8. Impact on actin cytoskeleton and cell shape of septin octamer sequestration by**  
1102 **microtubules via Sept9\_i1 MBD. a** Analysis of the presence of sub-nuclear actin fibers in  
1103 U2OS transfected by either siCtrl or siSept9. Results are from three independent experiments on  
1104 a total of 90 cells per condition (30 cells per experiments). Unpaired, two-tailed t-test with  
1105 Welch's correction, \*  $p < 0.05$ , \*\*  $p < 0.01$ , \*\*\*  $p < 0.0005$ , % of cells vs siCtrl. Right: Co-  
1106 localization of Sept7 with sub-nuclear actin stress fibers. White scale bar 10  $\mu\text{m}$ , insets: two-fold  
1107 zooms of frames region. **b** Analysis of the presence of sub-nuclear actin fibers in U2OS derived  
1108 cell lines stably expressing each one of the indicated C-terminally GFP tagged Sept9\_i1  
1109 constructs and the histone mCherry-H2B fusion. Results are from a single determination on 100  
1110 cell images per cell lines. **c** Analysis of shape changes on derived U2OS cell lines described in **b**  
1111 and adhering to medium size H micropatterns. d1: average maximum width of 35.170  $\mu\text{m}$   
1112 observed from measurement on four empty H micropatterns; d2: observed width of single  
1113 adherent cells at mid-maximal height of the H micropatterns. Representative images of merged  
1114 fluorescence channels of the three U2OS derived cell lines selected for analyses. Note that as for  
1115 the rest of the figure, these cell lines (U2OS.Sept9\_i1-GFP.mCherry-H2B, U2OS.Sept9\_i1-i5-  
1116 GFP.mCherry-H2B and U2OS.Sept9\_i1 $\Delta$ 1-25-GFP.mCherry-H2B) are indicated simply by the  
1117 originally transfected Sept9-GFP construct names. White scale bar is 10  $\mu\text{m}$ . Right:  
1118 measurements of the difference between d1 and d2 in cells from selected lines showing a higher  
1119 value when septins bind to microtubules, due to a reduction of the cell width at mid-maximal  
1120 height. Results are from two independent experiments on a total of 120 cells (60 cells per  
1121 experiment). Unpaired, two-tailed t-test with Welch's correction, \*\*\*  $p < 0.0005$ , d1-d2 vs  
1122 Sept9\_i1 $\Delta$ 1-25. Red lines represent mean values  $\pm$  SEM. **d** Measurements of d1-d2, as described  
1123 in **c**, in U2OS cells transfected either by either siCtrl or siSept9 as described in **c** showing that  
1124 Sept9 KD reduced cell width at mid-maximal height. Results are from three independent  
1125 experiments on a total of 120 cells (40 cells per experiment). Unpaired, two-tailed t-test with  
1126 Welch's correction, \*\*\*  $p < 0.0005$ , d1-d2 vs siCtrl. Red lines represent mean values  $\pm$  SEM.

1127  
1128  
1129  
1130  
1131  
1132  
1133  
1134  
1135  
1136  
1137  
1138  
1139  
1140  
1141  
1142  
1143  
1144  
1145  
1146



Kuzmic et al. Figure 1

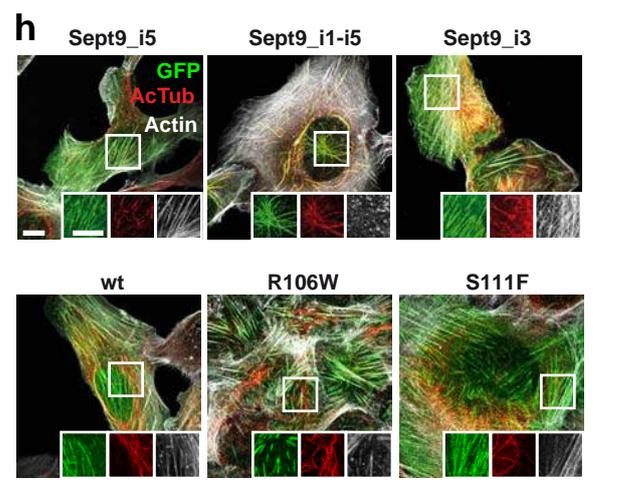
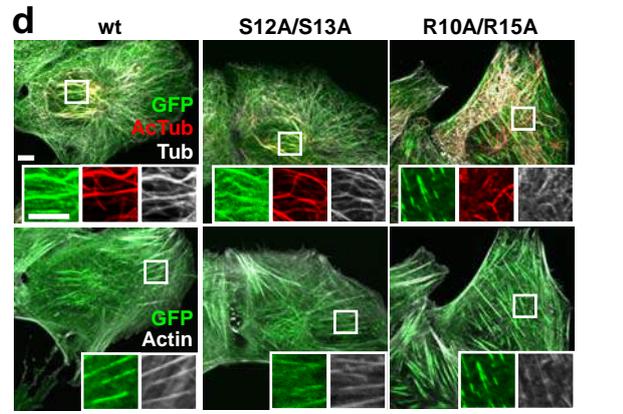
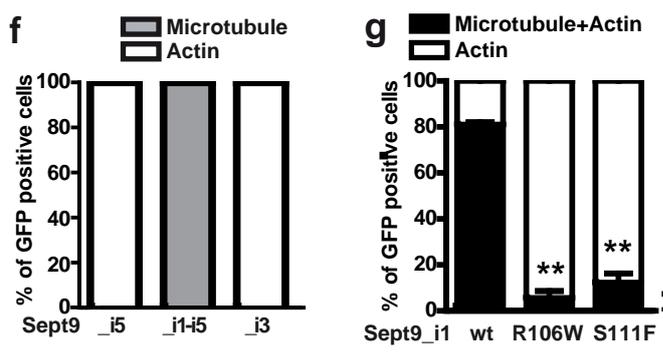
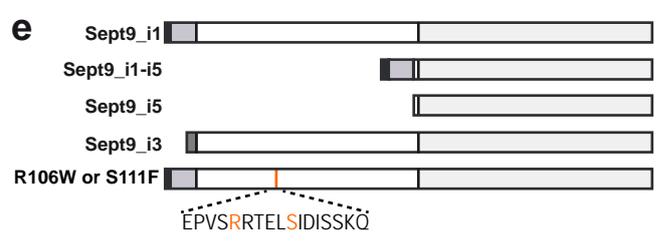
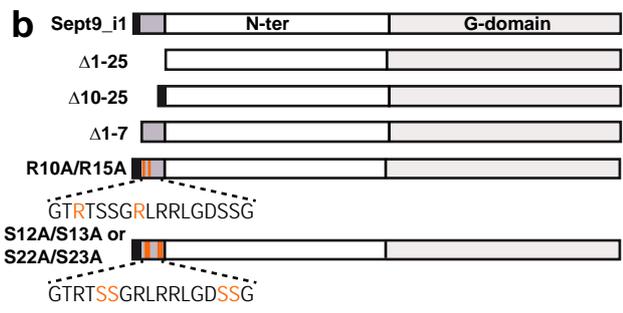
**a** Sept9\_i1 MAP-like MBD MAP4 R2-like AIR9-like  
 bioRxiv preprint doi: <https://doi.org/10.1101/2021.04.06.438596>; this version posted April 7, 2021. The copyright holder for this preprint (which was not certified by peer review) is the author/funder, who has granted bioRxiv a license to display the preprint in perpetuity. It is made available under aCC-BY-NC-ND 4.0 International license.

AIR9r2	S	V	S	V	S	S	K	-	R	A	A	S	T	K	K	-	K	P	V	I	S	S	N	L	I	K	P	T	A	-	S	S	S	L	R	V	S	G	T	T	P	V	T
AIR9r1	R	A	A	S	T	K	K	-	K	P	V	I	S	S	N	L	I	K	P	T	A	-	S	S	S	L	R	V	S	G	T	T	P	V	T								

Tau R1	R	L	Q	T	A	P	V	P	M	P	D	L	K	-	-	-	N	V	K	S	K	I	G	S	T	E	N	L	K	H	Q	P	G	G	G
Tau R2	K	V	Q	I	I	N	K	-	K	L	D	L	S	-	-	-	N	V	Q	S	K	C	G	S	K	D	N	I	K	H	V	P	G	G	G
Tau R3	S	V	Q	I	V	Y	K	-	P	V	D	L	S	-	-	-	K	V	T	S	K	C	G	S	L	G	N	I	H	H	K	P	G	G	G
Tau R4	Q	V	E	V	K	S	E	-	K	L	D	F	K	-	-	D	R	V	Q	S	K	I	G	S	L	D	N	I	T	H	V	P	G	G	G
MAP4 R1	S	R	L	A	T	N	T	S	A	P	D	L	K	-	-	-	N	V	R	S	K	V	G	S	T	E	N	I	K	H	Q	P	G	G	G
MAP4 R2	K	V	Q	I	V	S	K	-	K	V	S	Y	S	-	-	-	H	I	Q	S	K	C	G	S	L	D	N	I	K	H	V	P	G	G	G
MAP4 R3	N	V	Q	I	Q	N	K	-	K	V	D	I	S	-	-	-	K	V	S	S	K	C	G	S	K	A	N	I	K	H	K	P	G	G	G
MAP2 R1	Q	L	R	L	I	N	Q	P	L	P	D	L	K	-	-	-	N	V	K	S	K	I	G	S	T	D	N	I	K	Y	Q	P	K	G	G
MAP2 R3	Q	V	Q	I	V	T	K	-	K	I	D	L	S	-	-	-	H	V	T	S	K	C	G	S	L	K	N	I	R	H	R	P	G	G	G
MAP2 R4	R	V	K	I	E	S	V	-	K	L	D	F	K	-	-	E	K	A	Q	A	K	V	G	S	L	D	N	A	H	H	V	P	G	G	G

modeled Tau R2<sup>46</sup>  
 modeled Tau R1<sup>42</sup> or MAP4 R1<sup>47</sup>



Kuzmic et al. Figure 2



